

Copyright
by
Omneya Nassar
2019

**The Dissertation Committee for Omneya Nassar Certifies that this is the approved
version of the following dissertation:**

Thermodynamics of Ligand Binding to Glutamate Dehydrogenase

Committee:

B. Montgomery Pettitt, PhD
Supervisor, Chair

Thomas J. Smith, PhD

Yuriy Fofanov, PhD

Jia Zhou, PhD

Whitney Yin, PhD

Robert Fox, PhD

Thermodynamics of Ligand Binding to Glutamate Dehydrogenase

by

Omneya Nassar, B.S.

Dissertation

Presented to the Faculty of the Graduate School of

The University of Texas Medical Branch

in Partial Fulfillment

of the Requirements

for the Degree of

Doctor of Philosophy

The University of Texas Medical Branch

March, 2019

Dedication

To my mentor, Dr. B. Montgomery Pettitt, who is always committed to my success and bringing out the best in me. To my lab mates for their support and insightful discussions. To my mother (Eyman), father (Mohamed), older brother (Ahmed), twin brother (Riad), uncle (David), cousin (Kyrillos) and my grandfather (Dr. Ahmed Elnimr) for their never-ending support and encouragement.

Acknowledgements

Dr. B. Montgomery Pettitt is a phenomenal mentor and the author is forever grateful for the encouragement, support, autonomy, education and resources Dr. Pettitt has provided. The author would also like to thank collaborators Dr. Thomas Smith and Zoe Hoffpauir as well as lab members Dr. Gillian Lynch, Dr. Kai-Yui (Clem) Wong, Ms. Angelina Johnson, Dr. Cheng Zhang, Dr. Olga Samoylova, Dr. Cecilia Bores, Dr. Riley Workman, Danielle Seckfort, Dr. Kippi Dyer, Dr. Robert Harris, Dr. Karon Cassidy, Dr. Justin Drake, Dr. Heather Lander, and Ms. Brenda Boyko and for their collaboration and insightful discussions. These individuals created an intellectual and professional environment that is enriching to the pre-doctoral experience.

A special thank you to the author's family for their never-ending support and compassion. Mohamed and Eyman Nassar went above and beyond their parental roles and were essential for the success of the author. Ahmed and Riad Nassar were incredibly supportive and always made time to listen and address the concerns of the author. David Salib's encouragement and support is invaluable to the author, and the author will never forget the incredible effort he made to care for the author. Dr. Ahmed Elnimr, may he rest in peace, was a loving and brilliant grandfather who never hesitated to share his positive impressions of the author with everyone he knew.

The author would also like to thank her friends, Monica Garza, Jordan Fauser, Mai-Anh Van-Dinh, and Dr. Joseph Tang for their support and friendship. Their words of encouragement and entertaining conversations with the author were revitalizing.

Thermodynamics of Ligand Binding to Glutamate Dehydrogenase

Publication No. _____

Omneya Nassar, Doctor of Philosophy

The University of Texas Medical Branch, 2019

Supervisor: Bernard Montgomery Pettitt

The role of glutamate dehydrogenase (GDH) in disease has been exhibited in congenital hyperinsulinism, specifically, hyperinsulinism/hyperammonemia syndrome (HHS). GDH catalyzes the reversible deamination of glutamate to 2-oxoglutarate. Mutations in GDH can lead to GDH over activity, causing increased ATP production via the Krebs Cycle and excess insulin release. In addition, GDH over activity leads to depletion of glutamate, which is the source of the urea cycle precursor N-acetylglutamate. Reduction of N-acetylglutamate leads to reduced urea cycle activity and increased accumulation of ammonium. There are currently no treatments that directly target GDH and HHS patients are only treated symptomatically. To address the need to develop HHS therapeutics that directly target GDH, we began a computational investigation of the mechanism of allosteric ligand binding to GDH. During our computational investigation, we discovered a 40-year-old sequence error at the NADH/ADP/ECG binding site. Residue 387 was mistakenly identified as asparagine rather than the correct amino acid identity, lysine. The free energy penalty for the endogenous NADH ligand binding at the site having the incorrect residue was +5 kcal/mol per binding site. On correcting the sequence error our collaborators noticed improved refinement and electron density of the

ligands at the NADH/ADP/ECG site, which led us to continue our investigation of the difference in NADH (inhibitor) versus ADP (activator) binding at the NADH/ADP/ECG site. The computed binding free energy difference using thermodynamic integration is -0.3 kcal/mol, which is within the -0.275 and -1.7 kcal/mol experimental binding free energy difference range thereby allowing for postulation of how the structural changes induced in GDH between the two ligands causes the switch from inhibitor to activator. Visual analysis of the structural conformations agree with some structural findings of ligand-GDH interactions but also challenge other interactions. Our computational findings can serve as a hypothesis generator for experimentalists and guide them in both drug design and in prioritizing mutations when further investigating allosteric ligand binding to GDH.

TABLE OF CONTENTS

List of Tables	x
List of Figures	xi
List of Illustrations	xiii
List of Abbreviations	xiv
INTRODUCTION.....	1
Chapter 1 <i>Glutamate Dehydrogenase: Role in Disease and Biochemical Profile</i>	1-12
Hyperinsulinism/Hyperammonemia Syndrome	1-3
Hyperinsulinism Mechanism	2
Hyperammonemia Mechanism	3
Structure	3-5
Function	5
Regulation	5-9
References	10-12
Chapter 2 <i>Computational Approach</i>	13-20
Molecular Dynamics	13-14
Free Energy Calculations	14-18
Free Energy Perturbation	14-15
Thermodynamic Integration	15
Alchemical Transformation Method/Thermodynamic Cycle	16-17
Finite Size Effects	17-18
Supercomputing	18-19
Referecences	20

COMPUTATIONAL INVESTIGATION OF GLUTAMATE DEHYDROGENASE21

Chapter 3 *Glutamate Dehydrogenase: Structure of a Hyperinsulinism Mutant, Corrections to the Atomic model, and Insights into a Regulatory Site.*.....21-52

Abstract.....	22
Broader Audience Abstract.....	23
Introduction.....	24-26
Materials and Methods.....	26-
Structure determination of the H454Y-huGDH mutant.	26-27
Sequence Analysis	27
Model Refinement	27-28
Free Energy Simulation	29-30
Results.....	31-46
Structure of H454Y Mutant.....	31-33
Electron Density versus Protein Sequence	34-35
Evidence for the Sequence Error in Electron Density	35-36
Computed Free Energy Penalty	36-37
Structural Analysis of the NADH/ADP/ECG Site	37-46
Discussion and Conclusions	47-48
References.....	49-51
Acknowledgements.....	52

Chapter 4 *Allosteric Discrimination at the NADH/ADP Regulatory Site of Glutamate Dehydrogenase.*.....53-75

Abstract.....	54
Introduction.....	55-58
Methods	59-60
Software	59
Ligand System	59
Protein-Ligand Complex System.....	59-60
Free Energy Calculations	60
Results and Discussion	61-70
Binding Free Energy Calculation	61-64
Structural Analysis of Conformational Changes	64-70

Conclusion	70
Acknowledgements.....	71
Referecences	72-75
SUMMARY AND FUTURE DIRECTIONS.....	76-79
APPENDICIES	76-86
Appendix A Chapter 3 Supplemental Information	80-83
Appendix A1	80
Appendix A2.....	81
Appendix A3.....	82
Appendix A4.....	83
Appendix B Chapter 4 Supplemental Information	84-89
Appendix B1	84
Appendix B2.....	85
Appendix B3.....	86
Appendix B4.....	87
Appendix B5.....	87
Appendix B6.....	88-89
Vita	90

List of Tables

Table 3.1:	Data collection and refinement statistics	32
Table 3.2:	Distances (Å) between residue 387 and ligand in NADH binding pocket in the incorrect bovine GDH, correct bovine GDH, and H454Y mutant human GDH.....	35
Table 3.3:	Binding Free Energy differences in kcal/mol for the trimer with summed window errors using BSE n=1000	37
Table 4.1:	Computed binding free energy differences compared to experimental binding free energy differences	61
Table 4.2:	Total error and errors per lambda window for $\Delta G1$ and $\Delta G3$ calculated using the block standard error method.....	62
Table 4.3:	RMSD comparison of crystallographic GDH open conformation (pdb 6DHK) and simulation relative to GDH closed conformation (pdb 6DHD) at different regions of GDH	66

List of Figures

Figure 1:	Structure of GDH.....	4
Figure 1.2:	Monomer with GTP, ADP, NADH, and NAD ⁺ bound at their respective sites	7
Figure 1.3:	Residues in GDH associated with HHS when mutated	9
Figure 2.1:	Example thermodynamic cycle. A is the wild type protein and A* is the mutant protein	17
Figure 3.1:	View of bovine GDH trimer in the inhibited state bound to NADH. NADH bound at the second site	25
Figure 3.2:	Structure of the HHS H454Y mutant.....	33
Figure 3.3:	Comparison of asparagine and lysine in 3MW9 electron density at residue 387	35
Figure 3.4:	Thermodynamic cycle used to calculate the binding free energy difference of asparagine versus lysine as residue 387	36
Figure 3.5:	Electron density for the re-refined ligands bound to the NADH/ADP/ECG site.....	38
Figure 3.6:	Re-refined binding environments for NADH, ADP, and ECG	39
Figure 3.7:	GDH conformational changes upon ligand binding	43-44
Figure 3.8:	Surface details of the NADH/ADP/ECG binding site	46

Figure 4.1: Structure of GDH in the trimeric form bound to three NADH molecules at the NADH/ADP binding site	57
Figure 4.2: Free energy calculations using thermodynamic integration (TI) per λ intermediate	63
Figure 4.3: Computed relative binding free energy difference, $\Delta\Delta G$, of the alchemical conversion of NADH to ADP bound and unbound to GDH using TI..	64
Figure 4.4: RMSD comparison of crystallographic GDH open conformation (pdb 6DHK) relative to GDH closed conformation (pdb 6DHD).....	66
Figure 4.5: ADP interactions at each NADH/ADP binding site	68
Figure 4.6: NADH binding at the NADH/ADP site.....	69
Figure 5.1: Thermodynamic cycle to compute free energy penalty of S393I mutation in the presence of a native ligand, such as ADP or GTP	77
Figure 5.2: Thermodynamic Cycles Used to Calculate Binding Free Energy Differences ($\Delta\Delta G$).....	78

List of Illustrations

Illustration 1: Hyperinsulinism Mechanism.....	2
Illustration 2: Hyperammonemia Mechanism.....	3

List of Abbreviations

UTMB	University of Texas Medical Branch
GSBS	Graduate School of Biomedical Science
TDC	Thesis and Dissertation Coordinator
GDH	Glutamate Dehydrogenase
HHS	Hyperinsulinism/Hyperammonemia Syndrome
NAD ⁺	Nicotinamide Adenine Dinucleotide (oxidized)
NADH	Nicotinamide Adenine Dinucleotide (reduced)
GTP	Guanosine Triphosphate
ATP	Adenosine Triphosphate
ADP	Adenosine Diphosphate
FEP	Free Energy Perturbation
TI	Thermodynamic Integration
TACC	Texas Advanced Computing Center
CPU	Central Processing Unit
NAMD	Nanoscale Molecular Dynamics

INTRODUCTION

Chapter 1

Glutamate Dehydrogenase: Disease and Structure

Abstract

Mutations in glutamate dehydrogenase are associated with insulin-related disorders, specifically hyperinsulinism/hyperammonemia syndrome. Targeting glutamate dehydrogenase with agonists and antagonists can serve as potential therapeutics in treating diabetes type II and congenital hyperinsulinism. However, progress in developing therapeutics has been limited by the complex regulation of glutamate dehydrogenase. Thus, using computational techniques, we provide some insight and models that may address this impediment.

HYPERINSULINISM/HYPERAMMONEMIA SYNDROME

The most common cause of hypoglycemia in infants and young children is congenital hyperinsulinism, which is a condition that causes abnormally high levels of insulin in individuals.¹ Congenital hyperinsulinism is associated with mutations in four genes: SUR1, KIR6.2, GCK and GLUD1. Genes SUR1 and KIR6.2 encode the sequence for ATP-regulated potassium channel.¹ Patients require an autosomal recessive inheritance of mutations in SUR1 and/or KIR6.2 to exhibit the hypoglycemic phenotype of congenital hyperinsulinism. Gene GCK encodes islet glucokinase and gene GLUD1 encodes glutamate dehydrogenase 1 (GDH).¹ Individuals with autosomal dominant inheritance of mutations in GCK or GLUD1 exhibit the hypoglycemic phenotype of congenital Hyperinsulinism.¹

Individuals with point mutations in GDH can also have an asymptomatic 2-to-5 fold increase in plasma ammonia (hyperammonemia) in addition to protein-stimulated hypoglycemia.² These individuals have ammonia blood levels around 100 $\mu\text{mol/L}$, which is significantly higher than normal blood levels of ammonia of $<35 \mu\text{mol/L}$.² Thus, patients

with point mutations in GDH show a unique form of congenital hyperinsulinism known as hyperinsulinism/hyperammonemia syndrome or HHS.²

GDH catalyzes the reversible conversion of glutamate to 2-oxoglutarate in the presence of coenzyme nicotinamide adenine dinucleotide (NAD⁺). Guanosine triphosphate (GTP) is the major inhibitor of GDH. Mutations in the GTP binding site result in loss of GTP inhibition and GDH overactivity. This GDH overactivity is linked to HHS.³

Hyperinsulinism Mechanism

Increased GDH activity results in excess 2-oxo-glutarate production. 2-oxo-glutarate feeds into the Tricarboxylic Acid Cycle (TCA) cycle and increases adenosine triphosphate (ATP) production.⁴ Elevated levels of ATP bind to ATP-regulated potassium channels and closing of the ATP-regulated potassium channels occurs.⁴ This results in depolarization of beta cell and influx of calcium into the cell.⁴ The binding of calcium to microfilaments binding insulin causes a release of insulin from the beta cells.⁴ Thus, the persistent production of 2-oxo-glutarate caused by GDH overactivity results in excess insulin production and severe hypoglycemia in HHS patients.⁴

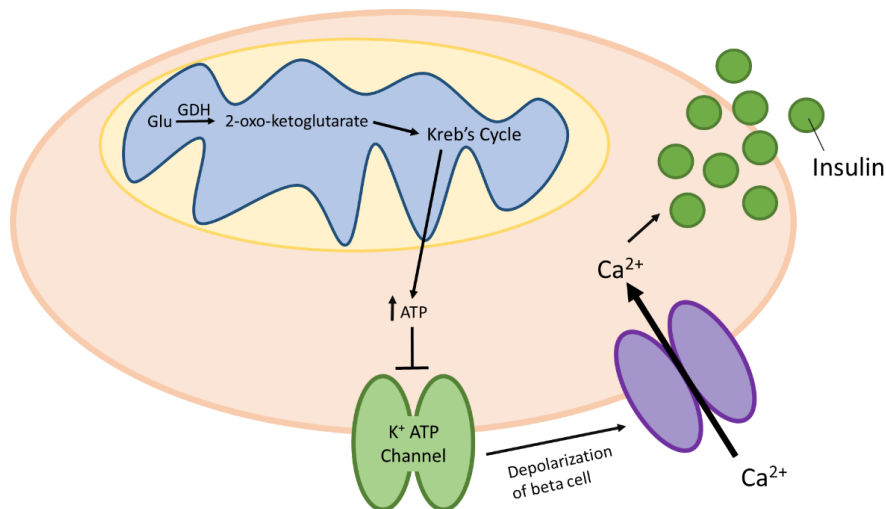


Illustration 1: *Hyperinsulinism Mechanism* Mechanism of insulin release in beta cells in the islets of Langerhans of the pancreas via glutamate dehydrogenase metabolism of glutamate.

Hyperammonemia Mechanism

Because GDH utilizes glutamate to produce 2-oxo-glutarate, GDH overactivity results in a depletion of glutamate.⁵ The depletion of glutamate halts the synthesis of N-acetylglutamate.⁵ N-acetylglutamate reacts with ammonia in the presence of carbamoyl phosphate synthetase 1 to form carbamoyl phosphate.⁵ The initiation of the urea cycle requires the catalyst N-acetylglutamate to react with ammonia to form the urea cycle initiator carbamoyl phosphate.⁵ Thus, without N-acetylglutamate, the urea cycle halts and ammonia accumulates in the body.⁵

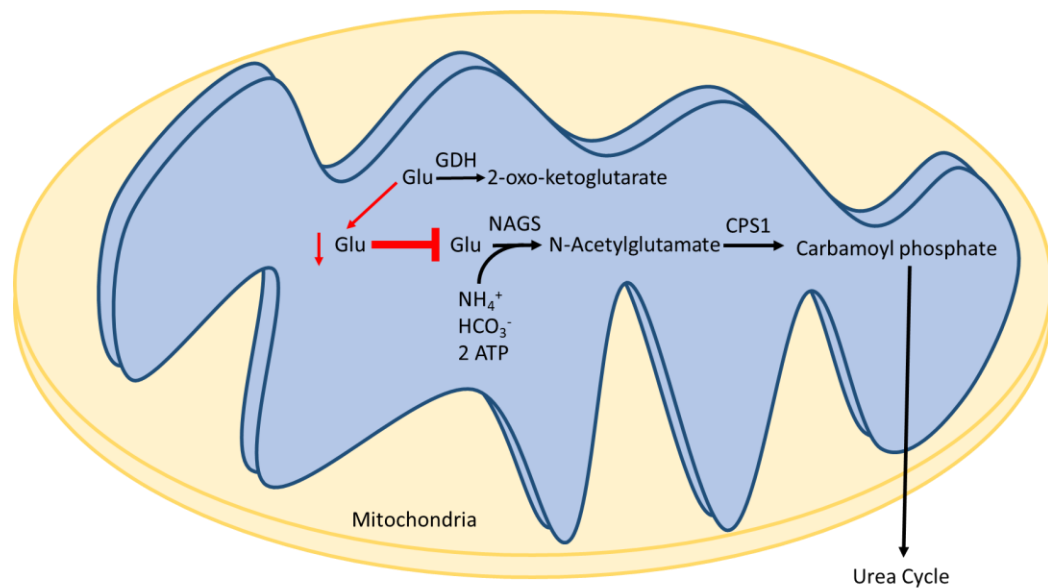


Illustration 2: *Hyperammonemia Mechanism* Mechanism of hyperammonemia in HHS patients. Excessive GDH activity depletes source of glutamate for N-acetylglutamate production. Lack of N-acetylglutamate production results in accumulation of ammonia in the cell.

STRUCTURE

Mammalian glutamate dehydrogenase (GDH) is a homohexameric enzyme with each monomer composed of approximately 500 residues.⁶⁻¹⁰ The assembly of GDH involves three monomers interacting to form a trimer.^{6, 11, 12} The trimer then dimerizes

with another trimer to form the homohexameric complex^{6, 9, 11, 12}. The two trimers have extensive interactions and form a core at the center of the protein.^{9, 11} Each monomer contains the following structures: coenzyme (NAD) binding domain, catalytic mouth, pivot helix, antenna helix, GTP binding site, ADP binding site, and pigtail helix.^{7, 11-18} The antenna is a structure unique to mammalian GDH and is proposed to be involved in the regulation of the enzyme.^{6, 9, 11, 13, 19} To summarize, each homohexamer is a dimer of trimers that has a total of 6 NAD binding domains, 6 catalytic mouths, 6 pivot helices, 6 GTP binding sites, 6 ADP binding sites, 6 pigtail helices, 6 antennae, and 1 core. Glutamate dehydrogenase is a highly conserved enzyme across all organisms on Earth.⁶ Moreover, human isoforms are highly similar to bovine GDH. Bovine GDH has 81% sequence identity with GDH (NCBI Blast). See Figure 1 for the structure of GDH.

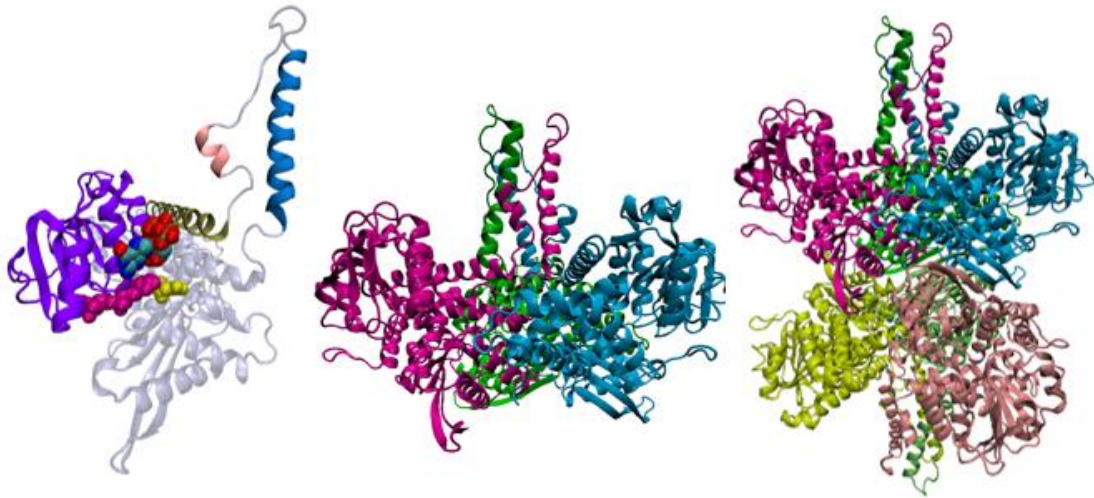


Figure 1: Structure of GDH. On the left is the monomer with each colored structure or ligand: antenna (blue), pigtail (pink), pivot helix (gold), NAD binding domain (purple), GTP (colored by atom), NAD⁺ (magenta), glutamate (yellow). In the center is the trimer with each monomer colored in blue, green or magenta. On the right is the hexamer (dimer of trimers) with each monomer colored in blue, magenta, green, yellow, pink and lime.

Each monomer has an antenna, NAD⁺ binding domain, pivot helix, glutamate binding domain, and GTP binding site. The NADH binding site is located between the

subunits (6 sites per hexamer). The catalytic site is comprised of the NAD⁺ binding domain and glutamate binding domain. The residues involved in NAD⁺ and glutamate binding include Q330, S276, E275, N254, V255, R211, K126, S381, K90, K114, N349, A326, N169, and S170. The GTP binding site is located adjacent to the NAD⁺ binding domain and is composed of residues Y262, R217, R265, R261, H209, H450, and H258. The ADP binding site is located on the opposite side of the GTP binding site and adjacent to the NAD⁺ binding domain. The ADP binding site is composed of residues R459, R396, S393, K387, D119, R86, and H85.⁸ See Figure 1.2 for a depiction of these sites.

FUNCTION

GDH catalyzes the deamination of glutamate in the presence of the coenzyme NAD or NADP to produce 2-oxoglutarate and ammonium.^{6, 13, 21-23} The proposed mechanism of catalysis is as follows: glutamate binds into the open catalytic mouth with slight preference over coenzyme binding, underneath the NAD binding domain.⁶ The coenzyme binds at the NAD binding domain surface located above glutamate.⁶ The binding of NAD induces the NAD binding domain to rotate approximately 18 degrees and firmly close the catalytic mouth down on glutamate and the coenzyme.⁶ As the mouth closes, the bottom of each antenna helix rotates out counter-clockwise and appears to push against the pivot helix.⁶ The pigtail, located in the descending loop of the antenna, expands and shortens as the mouth closes.⁶ The pivot helix rotates counter-clockwise along the helical and trimer threefold axes.⁶ Finally, the core compresses as the trimers come closer together and the hexamer 'exhales' as the mouth closes.⁶

REGULATION

The two most commonly described regulators of GDH are guanosine triphosphate (GTP) and adenosine diphosphate (ADP).^{6, 12, 13, 24-26} The GTP binding site is located at

the "jaw" of each subunit (see Figure 1.2).⁶ The jaw is the space located between the NAD binding domain and the pivot helix.⁶ When the NAD binding domain closes, the space of the GTP binding site increases.⁶ This allows GTP to interact with GDH via its triphosphate group and prevents product release from occurring.^{6, 12, 25, 27} In contrast, the ADP binding site is located underneath the pivot helix and behind the NAD binding domain.^{6, 12, 13} It seems unexpected to have ADP bind in an area that locks the pivot helix in place. However, mutational studies have revealed that ADP interacts with the basic residue R463 on the pivot helix to assist in opening the catalytic mouth.¹³ It was found that if R463 is mutated to alanine, the enzyme is not activated by ADP even though ADP can still bind at the same site.¹³ The differences in the way GTP and ADP interact with GDH explains how they may antagonistically affect each other's binding sites but also have opposite effects on the NAD binding domain.⁶

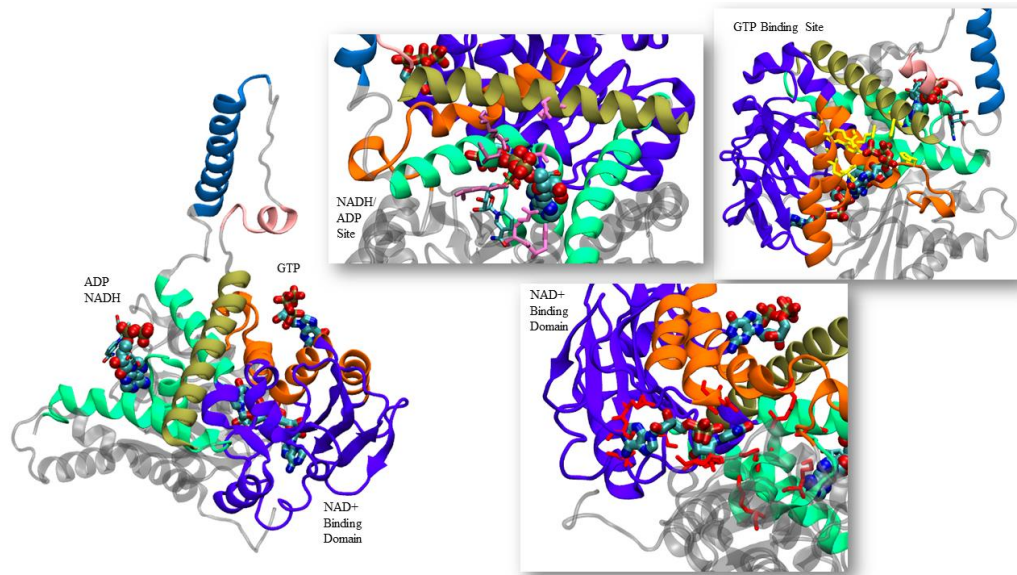


Figure 1.2: Monomer with GTP, ADP, NADH, and NAD⁺ bound at their respective sites. As depicted above, GTP and ADP/NADH are on opposite sides of the pivot helix (gold). GTP binding site is located in the jaw region (orange) and pivot helix with residues in yellow. The NAD⁺ binding site is located adjacent and under the jaw region with residues colored in red. The ADP/NADH binding site is colored in green and also involves the pivot helix. All ligands are colored by atom.

Nevertheless, both GTP and ADP act as energy measures and regulate GDH by sensing the energy state of the mitochondria.^{6, 12} When in a high-energy state, the wealth of triphosphates make the GDH inhibition more favorable.^{6, 12, 28} In contrast, when in a low energy state, the higher levels of ADP activates GDH to produce 2-oxoglutarate and promote the activity of the Krebs cycle.^{6, 12, 28} The current hypothesis of GDH allosteric regulation is that GDH is kept in a tense state while the subtle fluctuations in the ADP:GTP ratios adjust GDH activity.⁶ Other allosteric inhibitors and activators include palmitoyl-coA, NADH, ATP, diethylstilbestrol, zinc, and leucine, beta-2-aminobicyclo[2,2,1]-heptane-2-carboxylic acid (BCH), ADP, respectively.⁶

Mammalian glutamate dehydrogenases have several actively acetylated lysine residues.²⁹ The most reactive lysine sites on bovine glutamate dehydrogenase are K503,

K480, and K477.²⁹ Each monomer has a K503 residue, which is located near the GTP binding site.²⁹ This lysine residue is known to undergo acetylation at a second order rate of $757.85 \times 10^{-5} \text{ M}^{-1} \text{ s}^{-1}$ to inactivate GDH.²⁹ The K480, K477, and K480 residues are located on the trimeric antennae and are acetylated at a second order rate of $205.79 \times 10^{-5} \text{ M}^{-1} \text{ s}^{-1}$ inactivate GDH.²⁹

There are several mutations found in GDH that lead to its overactivity and inevitably result in hyperinsulinism/hyperammonemia syndrome in patients. These mutations are found around the GTP binding site (H262, R265, Y266, R269, R221, H454, and K450), in the pivot helix (H454, K450, and S448), between the pivot helix and pigtail (A447, G446, and S445), in the pigtail (Q441 and F440), and in the antenna (L413 and N410).^{6, 30-32} See Figure 1.3 for a depiction of residues involved in HHS.

HHS Mutations

GTP Binding Site: R221, H262, R265, Y266, R269, H454, K450

Pivot Helix: H454, K450, S448

Region Between Pivot Helix and Pigtail: A447, G446, S445

Pigtail: Q441, F440

Antenna: L413, N410

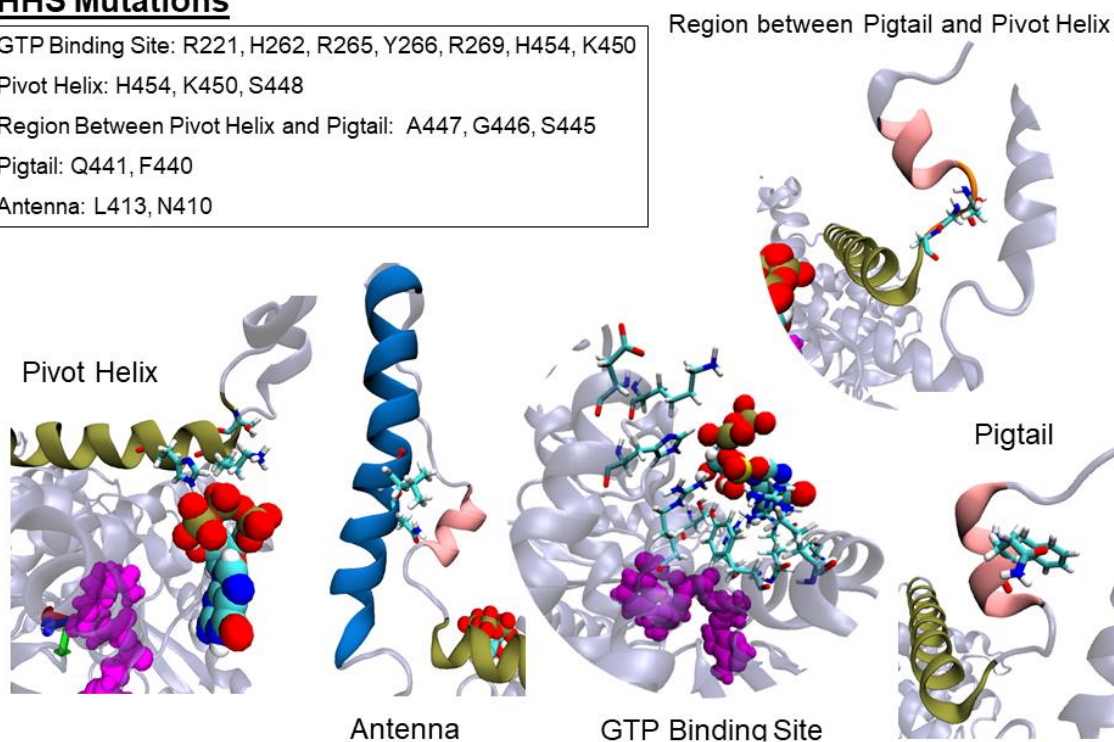


Figure 1.3: Residues in GDH associated with HHS when mutated.

We are interested in understanding native ligand binding sites and their relation to GDH activity to provide insight in GDH therapeutic development. While this discussion of GDH-ligand binding may seem simple, there are some phenomena that we would like to investigate. For example, in Chapter 2, we identify an important residue in ligand binding that was previously misidentified and its relation to the NADH/ADP/ECG binding site. In Chapter 4, we discuss why the NADH/ADP site could have both inhibitory and agonistic effects depending on the ligand bound. However, before discussing our experiments, I provide a brief introduction to computational chemistry in Chapter 2, where I will discuss common computational procedures to model protein-ligand binding and computing binding free energies.

References

1. MacMullen C, Fang J, Hsu BY, et al. Hyperinsulinism/hyperammonemia syndrome in children with regulatory mutations in the inhibitory guanosine triphosphate-binding domain of glutamate dehydrogenase. *J Clin Endocrinol Metab.* 2001;86:1782-1787.
2. Weinzimer SA, Stanley CA, Berry GT, Yudkoff M, Tuchman M, Thornton PS. A syndrome of congenital hyperinsulinism and hyperammonemia. *J Pediatr.* 1997;130:661-664.
3. Fang J, Hsu BY, MacMullen CM, Poncz M, Smith TJ, Stanley CA. Expression, purification and characterization of human glutamate dehydrogenase (GDH) allosteric regulatory mutations. *Biochem J.* 2002;363:81-87.
4. Stanley CA. Regulation of glutamate metabolism and insulin secretion by glutamate dehydrogenase in hypoglycemic children. *Am J Clin Nutr.* 2009;90:862S-866S.
5. Huijmans JG, Duran M, de Klerk JB, Rovers MJ, Scholte HR. Functional hyperactivity of hepatic glutamate dehydrogenase as a cause of the hyperinsulinism/hyperammonemia syndrome: effect of treatment. *Pediatrics.* 2000;106:596-600.
6. Smith TJ, Stanley CA. Untangling the glutamate dehydrogenase allosteric nightmare. *Trends in biochemical sciences.* 2008;33:557-564.
7. Baker PJ, Britton KL, Engel PC, et al. Subunit assembly and active site location in the structure of glutamate dehydrogenase. *Proteins: Structure, Function, and Bioinformatics.* 1992;12:75-86.
8. Banerjee S, Schmidt, T., Fang, J., Stanley, C.A. and Smith, T.J. Structural studies on ADP activation of mammalian glutamate dehydrogenase and the evolution of regulation. *Biochemistry.* 2003;42:10.
9. Smith HQ, Li C, Stanley CA, Smith TJ. Glutamate Dehydrogenase, a Complex Enzyme at a Crucial Metabolic Branch Point. *Neurochem Res.* 2017.
10. Moon K, Piskiewicz, D. and Smith, E.L. Glutamate dehydrogenase: amino-acid sequence of the bovine enzyme and comparison with that from chicken liver. *Proceedings of the National Academy of Sciences.* 1972;69:3.
11. Peterson PE, Smith TJ. The structure of bovine glutamate dehydrogenase provides insights into the mechanism of allostery. *Structure.* 1999;7:769-782.

12. Li M, Li C, Allen A, Stanley CA, Smith TJ. Glutamate dehydrogenase: structure, allosteric regulation, and role in insulin homeostasis. *Neurochem Res*. 2014;39:433-445.
13. Banerjee S, Schmidt T, Fang J, Stanley CA, Smith TJ. Structural studies on ADP activation of mammalian glutamate dehydrogenase and the evolution of regulation. *Biochemistry*. 2003;42:3446-3456.
14. Bell E, Bell JE. Catalytic activity of bovine glutamate dehydrogenase requires a hexamer structure. *Biochemical Journal*. 1984;217:327-330.
15. George A, Bell JE. Effects of adenosine 5'-diphosphate on bovine glutamate dehydrogenase: diethyl pyrocarbonate modification. *Biochemistry*. 1980;19:6057-6061.
16. Pal PK, Colman RF. Affinity labeling of an allosteric GTP site of bovine liver glutamate dehydrogenase by 5'-p-fluorosulfonylbenzoylguanosine. *Biochemistry*. 1979;18:838-845.
17. Plaitakis A, Metaxari M, Shashidharan P. Nerve tissue- specific (GLUD2) and housekeeping (GLUD1) human glutamate dehydrogenases are regulated by distinct allosteric mechanisms: implications for biologic function. *Journal of neurochemistry*. 2000;75:1862-1869.
18. Prough RA, Culver JM, Fisher HF. The mechanism of activation of glutamate dehydrogenase-catalyzed reactions by two different, cooperatively bound activators. *J Biol Chem*. 1973;248:8528-8533.
19. Li C, Li M, Chen P, et al. Green tea polyphenols control dysregulated glutamate dehydrogenase in transgenic mice by hijacking the ADP activation site. *J Biol Chem*. 2011;286:34164-34174.
20. Geer LY, Marchler-Bauer A, Geer RC, et al. The NCBI BioSystems database. *Nucleic Acids Res*. 2010;38:D492-496.
21. Li M, Li CH, Allen A, Stanley CA, Smith TJ. The structure and allosteric regulation of mammalian glutamate dehydrogenase. *Archives of Biochemistry and Biophysics*. 2012;519:69-80.
22. FRIEDEN C. GLUTAMATE DEHYDROGENASE. V. THE RELATION OF ENZYME STRUCTURE TO THE CATALYTIC FUNCTION. *J Biol Chem*. 1963;238:3286-3299.
23. Syed SE, Engel PC, Parker DM. Functional studies of a glutamate dehydrogenase with known three-dimensional structure: steady-state kinetics of the forward and reverse reactions catalysed by the NAD(+)-dependent glutamate dehydrogenase of *Clostridium symbiosum*. *Biochim Biophys Acta*. 1991;1115:123-130.

24. Wrzeszczynski KO, Colman RF. Activation of bovine liver glutamate dehydrogenase by covalent reaction of adenosine 5'-O-[S-(4-bromo-2, 3-dioxobutyl) thiophosphate] with arginine-459 at an ADP regulatory site. *Biochemistry*. 1994;33:11544-11553.
25. Dieter H, Koberstein R, Sund H. Studies of glutamate dehydrogenase. The interaction of ADP, GTP, and NADPH in complexes with glutamate dehydrogenase. *Eur J Biochem*. 1981;115:217-226.
26. Lord K, De León DD. Monogenic hyperinsulinemic hypoglycemia: current insights into the pathogenesis and management. *Int J Pediatr Endocrinol*. 2013;2013:3.
27. Koberstein R, Sund H. Studies of glutamate dehydrogenase. The influence of ADP, GTP, and L-glutamate on the binding of the reduced coenzyme to beef-liver glutamate dehydrogenase. *Eur J Biochem*. 1973;36:545-552.
28. Kibbey RG, Choi CS, Lee HY, et al. Mitochondrial GTP insensitivity contributes to hypoglycemia in hyperinsulinemia hyperammonemia by inhibiting glucagon release. *Diabetes*. 2014;63:4218-4229.
29. Paz Z, García-Pedrajas MD, Andrews DL, Klosterman SJ, Baeza-Montañez L, Gold SE. One step construction of Agrobacterium-Recombination-ready-plasmids (OSCAR), an efficient and robust tool for ATMT based gene deletion construction in fungi. *Fungal Genet Biol*. 2011;48:677-684.
30. Bahi-Buisson N, Roze E, Dionisi C, et al. Neurological aspects of hyperinsulinism-hyperammonemia syndrome. *Dev Med Child Neurol*. 2008;50:945-949.
31. Stanley CA, Fang J, Kutyna K, et al. Molecular basis and characterization of the hyperinsulinism/hyperammonemia syndrome: predominance of mutations in exons 11 and 12 of the glutamate dehydrogenase gene. HI/HA Contributing Investigators. *Diabetes*. 2000;49:667-673.
32. Palladino AA, Stanley CA. The hyperinsulinism/hyperammonemia syndrome. *Rev Endocr Metab Disord*. 2010;11:171-178.

Chapter 2

Computational Approach

Abstract

The theoretical computation of binding free energies can involve a variety of techniques and a myriad of approaches. Some of the more common techniques used in this study as well as across the scientific community includes molecular dynamics sampling and alchemical transformation techniques such as free energy perturbation and thermodynamic integration.

MOLECULAR DYNAMICS

Molecular dynamics is a computational technique that utilizes statistical mechanics to bridge the gap between the macroscopic and microscopic states of a sample.¹ For this project, the macroscopic state of interest is the binding free energy difference while the microscopic states are the momenta and positions of the atoms within each GDH molecule. The free energy difference is a function of the potential energy of the system and the potential energy of the system is a function of the momenta and positions of a system in a particular state. The momenta and positions of the atoms are generated by integrating Newton's laws of motion.² A commonly used algorithm to integrate Newton's equations of motions is the Verlet algorithm.² The Verlet algorithm uses the atom's previous (time = $t-\delta t$) and current (time = t) positions and accelerations to determine the new positions in the future (time = $t + \delta t$).² Below is the derivation of the Verlet algorithm.

$$r(t+\delta t) = r(t) + v(t)\delta t + \frac{1}{2} a(t)\delta t^2 + \dots \quad (1)$$

$$r(t-\delta t) = r(t) - v(t)\delta t + \frac{1}{2} a(t)\delta t^2 - \dots \quad (2)$$

Add (1) and (2)

$$r(t+\delta t) + r(t-\delta t) = 2r(t) + a(t)\delta t^2$$

$$r(t+\delta t) = 2r(t) - r(t-\delta t) + a(t)\delta t^2 \quad (\text{Verlet Algorithm})$$

The velocities do not appear in the Verlet algorithm but can be computed by taking the difference of the future position and past position of the atoms and dividing by $2\delta t$.²

Thus, integrating Newton's equations of motions allows for the atomic positions and velocities to vary with time thereby producing trajectories with successive protein configurations.² Equation 3 shows the computation of velocity without using the Verlet Algorithm.

$$v(t) = [r(t+\delta t) - r(t-\delta t)]/2\Delta t \quad (3)$$

Initiation of molecular dynamics simulations require an initial configuration of the system of interest.² Initial structures can be experimentally determined structures or when no experimental structure exists, theoretical models predicted computationally by software such as MODELLER^{2,3}. Our studies used the more reliable crystal structures deposited in the Research Collaboratory for Structural Bioinformatics (RCSB) database. The resolution of the structures we usually hope to use is 2.5Å or better, which allows for structural observation of heavy atoms such as carbon, nitrogen, oxygen, sulfur and phosphate, but not for hydrogens. Thus, hydrogens were computationally added. Structures with higher resolutions are avoided for computational modeling.

FREE ENERGY CALCULATIONS

Because thermodynamics is state dependent and path independent, the use of non-physical intermediates can be implemented in free energy calculations and have shown to reproduce experimental values. Two common techniques to evaluate free energy calculations using alchemical transformations include free energy perturbation and thermodynamic integration.⁴

Free Energy Perturbation

The free energy perturbation (FEP) technique was introduced by Robert Zwanzig in 1954 and relates two free energy states to the weighted change in their potential energies by the Zwanzig equation⁵ (see equation 4):

$$\Delta G(A \rightarrow B) = G(B) - G(A) = -1/\beta \ln \langle \exp(-\beta(U_B - U_A)) \rangle \quad (4)$$

where $G(A)$ is the free energy of the initial state, $G(B)$ is the free energy of the final state, ΔG is the free energy difference between $G(A)$ and $G(B)$, β is the inverse Boltzmann

constant multiplied by the absolute temperature ($\beta = 1/k_B T$), U_A is the potential energy of the initial state and U_B is the potential energy of the final state. Note that the potential energy is a function of the system's positions.

Sampling the energies of only the initial and final states limits the number of conformations sampled in phase space thereby reducing the accuracy of the free energy difference calculations.⁴ In order to enhance sampling of the phase space of the states, the computation of the free energy difference can be divided into multiple intermediates, which are typically denoted by λ .⁴ The number of intermediates used can be unique for each system and are classically uniformly sampled for simplicity.⁴

Thermodynamic Integration

Like FEP, optimal calculation of the binding free energy difference using thermodynamic integration (TI) requires a thermodynamic path consisting of non-physical intermediates (λ).⁴ However, in contrast to FEP, the binding free energy computed using TI is accomplished by integrating the thermodynamic path from state A to state B.⁶ Equation (5) shows the relation of free energy to the thermodynamic path from state to state B.⁶ Integration can be approximated using the trapezoid method or Simpson's rule.

$$\Delta G(A \rightarrow B) = \int_A^B \langle U_A(\lambda) - U_B(\lambda) \rangle_\lambda d\lambda \quad (5)$$

TI can be related to FEP by taking the Taylor expansion of the exponent in the Zwanzig equation.

$$\Delta G = -k_B T \sum \ln \langle \exp(-\beta [U_{\lambda=i+1} - U_{\lambda=i}]) \rangle$$

$$\Delta G \cong -k_B T \sum \ln \langle (1 - \beta [U_{\lambda=i+1} - U_{\lambda=i}]) \rangle$$

$$\Delta G \cong \sum \langle U_{\lambda=i+1} - U_{\lambda=i} \rangle$$

Using this relationship, we can utilize the changes in potential energy computed from our FEP simulations and compute the TI binding free energy difference ($\Delta \Delta G_{TI}$) in addition to the FEP binding free energy difference ($\Delta \Delta G_{FEP}$).

Alchemical Transformation Method and Thermodynamic Cycles

While determining free energies of non-physical compounds in wet-lab experiments is impossible, theoretical computation of non-physical intermediates has proven to be an effective method of enhancing sampling and resulting in free energy calculations similar to those obtained experimentally. Because thermodynamics is dependent on the end states and independent of the path taken to the end state, using alchemical intermediates is a viable method to compute free energies.⁷

Alchemical intermediates are built depending on the approach used: dual topology or single topology.^{4,8} In the dual topology approach, one alchemical molecule contains two components: the appearing atoms of the end state and the disappearing atoms of the initial state. Both appearing and disappearing atoms are simultaneously present during the simulations and can only sense the environment, not each other. In the single topology approach, a molecule is either appearing or disappearing, but not both simultaneously as done in dual topology. In our free energy calculations, the dual topology method was used as it was determined to be the most optimal method for measuring free energies of ligand binding to GDH because single topology methods showed larger errors in our calculations.

In addition to using the dual topology or single topology methods, the decoupling of electrostatics and van der Waals energies can be accomplished.^{4, 9-11} Typically, the decoupling of the electrostatics and van der Waals energies produces values with smaller errors and we utilized this approach in our calculation of the binding free energy difference of N387K sequence error. However, we avoided decoupling the electrostatics and van der Waals components when computing the binding free energy difference of NADH versus ADP binding to GDH due to complications when sampling.

The computational schematic for computing binding free energies are thermodynamic cycles. In thermodynamic cycles, the initial state and end state are related by the alchemical transformation (horizontal legs) and the change in solvation between the

same initial or end state (vertical legs). See Figure 2.1 for an example of a thermodynamic cycle. Because one must end the same place as one started in the thermodynamic cycle, the sum of the components must equal zero. Thus, moving clockwise, one can determine the sign of each free energy component and sum the components to equal to zero. From there, one set the solvation (vertical leg) free energies to equal the alchemical transformation (horizontal) free energies and thus relate the binding free energy difference to the alchemical transformation free energies as well as the solvation free energies.

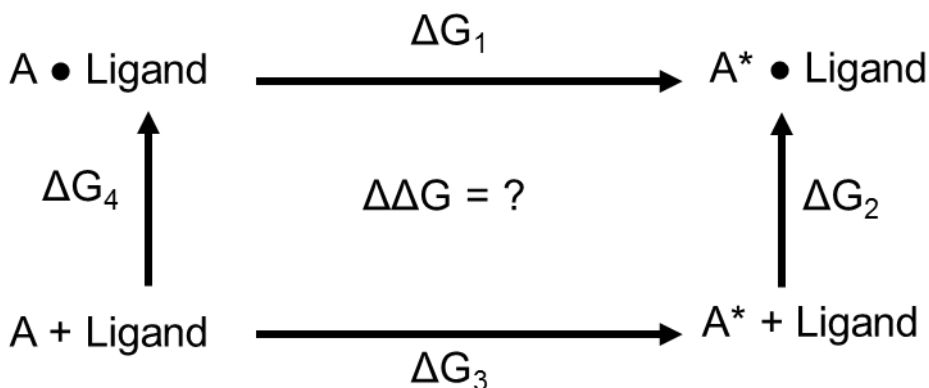


Figure 2.1: Example thermodynamic cycle. A is the wild type protein and A* is the mutant protein.

Finite Size Effects

As mentioned previously, the binding free energies are computed using the potential energy of the system. The potential energy of the system has both bonded and non-bonded components, one of which is the computation is the electrostatic component. Finite size effects are errors that arise when treating the long-range electrostatics using the Ewald method of a system in which the charge of the system changes.¹² While the charging free energy depends on the applied methodology, neglecting correction terms can impair the thermodynamic interpretation of protein-ligand interactions.¹² For example, when alchemically transforming an asparagine residue to a lysine residue, the charge of the

system gains a +1 charge from the lysine. Particle mesh Ewald method does not handle the long-range electrostatics of a non-neutral system well, thus, corrections have been included to address the errors that arise from conducting such computations.¹² Several of methods have been implemented in attempt to correct for finite size effects including a background neutralizing plasma, simultaneous ion mutations, twin simulations with opposite counter-ion mutations, numerical corrections and analytical corrections. The correction method chosen for our studies is the Hummer et al. correction¹², which is an analytical correction that has proven sufficient for both small ion and large protein complexes (see Equation 6).

$$\Delta G_{\text{correction}} = -\frac{1}{2} \zeta_{\text{Ewald}} (q_1^2 - q_0^2) \times 332 \quad (6)$$

SUPERCOMPUTING RESOURCES FOR COMPUTATIONAL BIOLOGY

Abstract

Because the computation of free energy requires computing the bonding and non-bonding potential energies of each atom, the memory and processing power of a desktop becomes inadequate when attempting to observe protein conformational changes in the presence or absence of ligands on the nanosecond to microsecond timescale. Thus, large-scale processors in supercomputers allow for large computations to be completed within days instead of months using parallel computing techniques.

TACC Supercomputing Center

The supercomputing resources utilized to compute binding free energy calculations were supercomputers Stampede2 and Lonestar5 at the Texas Advanced Computing Center (TACC) in Austin, TX.¹³ With Stampede 2, we have access to 4,200 Knights Landing (KNL) nodes and 1,736 Intel Xeon Skylake (SKX) nodes.¹³ Each KNL node contains 68 computer processing units (CPUs) and each SKX node contains 48 CPUs.¹³ Thus, we were able to compute microsecond trajectories of the N387K sequence error while using the KNL nodes in 48960 corehours.

Lonestar 5 was used for our second computational investigation, which compared NADH to ADP binding in GDH. We have access to 1,252 nodes in the Lonestar 5

supercomputer with each node containing 24 CPUs. Large systems, such as the solvated GDH-ligand complexes (~200,000 atoms), require 2 nodes with a total of 48 computer processing units (CPUs) to most efficiently complete runs within two weeks. Smaller systems, such as solvated ligand systems (~5,000 atoms), require 1 node and a total of 24 CPUs to complete within a few days. In addition to large processing power, supercomputers allow for temporarily storing data in the terabyte (TB) range. This allows for the extraction of large energy data sets as well as detailed visual inspection of trajectories.

The following chapters discuss our computational experiments used to model glutamate dehydrogenase interacting with native ligands, such as ADP and NADH. Chapter 3 discusses the importance and binding free energy penalty of a 40 year-old sequence error found in the bovine GDH sequence that is located in the NADH/ADP binding site. After identifying the error, the improved electron density and crystallographic structure of the ligands as well as the binding site led us to investigate the binding of both NADH and ADP at the NADH/ADP binding site (chapter 4). As mentioned previously in chapter 1, NADH at the NADH/ADP binding site acts as an inhibitor by preventing product release while ADP at the NADH/ADP binding site functions as an activator. Understanding the binding of both the activator (ADP) and inhibitor (NADH) can provide insight in understanding the functionality of an inhibitor or activator at the NADH/ADP site.

References

1. Allen MP, Tildesley DJ. *Computer simulation of liquids*: Oxford university press; 2017.
2. Leach AR. *Molecular modelling: principles and applications*: Pearson education; 2001.
3. Fiser A, Šali A. Modeller: generation and refinement of homology-based protein structure models. *Methods in enzymology*. 2003;374:461-491.
4. Chipot C, Pohorille A, Harvard. *Free energy calculations*: Springer-Verlag Berlin Heidelberg; 2007.
5. Zwanzig RW. High-temperature equation of state by a perturbation method. I. nonpolar gases. *The Journal of Chemical Physics*. 1954;22:1420-1426.
6. Straatsma TPaB, H.J.C. Free energy of ionic hydration: Analysis of a thermodynamic integration technique to evaluate free energy differences by molecular dynamics simulations. *The Journal of Chemical Physics*. 1988;89:5876-5886.
7. Lybrand TP, McCammon JA, Wipff G. Theoretical calculation of relative binding affinity in host-guest systems. *Proc Natl Acad Sci U S A*. 1986;83:833-835.
8. Kollman P. Free energy calculations: applications to chemical and biochemical phenomena. *Chemical Reviews*. 1993;93:2395-2417.
9. PA B, UC S, R L, PA K. Free energy calculations by computer simulation *Science*. 1987;236:564-568.
10. Mobley DL, Gilson MK. Predicting Binding Free Energies: Frontiers and Benchmarks. *Annu Rev Biophys*. 2017;46:531-558.
11. Chipot C, Mark AE, Pande VS, Simonson T. Applications of Free Energy Calculations to Chemistry and Biology. *Free Energy Calculations*. Vol 86: Springer; 2007:463-501.
12. Hummer G, Pratt LR, Garcia AE. Free energy of ionic hydration. *The Journal of Physical Chemistry*. 1996;100:1206-1215.
13. TACC - Texas Advanced Computing Center. Vol 2019. <https://www.tacc.utexas.edu>2011-2018.

COMPUTATIONAL INVESTIGATION OF GLUTAMATE DEHYDROGENASE

Chapter 3

Nassar OM, Li C, Stanley CA, Pettitt BM, Smith TJ. Glutamate dehydrogenase: Structure of a hyperinsulinism mutant, corrections to the atomic model, and insights into a regulatory site. *Proteins*. 2019;87:41–50. <https://doi.org/10.1002/prot.25620>

Glutamate Dehydrogenase: Structure of a Hyperinsulinism Mutant, Corrections to the Atomic model, and Insights into a Regulatory Site.

Omneya M. Nassar¹, Changhong Li³, Charles A. Stanley³, B. Montgomery Pettitt^{*1, 2}, and Thomas J. Smith^{*2}.

¹Department of Pharmacology and Toxicology, ²Department of Biochemistry and Molecular Biology, University of Texas Medical Branch, 301 University Blvd, Galveston, TX, 77555-0304

³Division of Endocrinology, The Children's Hospital of Philadelphia, Philadelphia, PA, 19104.

***Co-Corresponding Authors:**

B. Montgomery Pettitt
Tel: 409-772-0723
Email: mpettitt@utmb.edu

Thomas J. Smith
Tel: 409-772-6028
Email: thosmith@utmb.edu

Contributors:

Omneya Nassar found the N387K error and conducted the computational analysis. Dr. Thomas Smith provided the H454Y crystal mutant structure, redeposited corrected structures and provided structural analysis of NADH/ADP binding pocket. Dr. Changhong Li and Dr. Charles A. Stanley contributed to the mutant crystal structure determination.

Running Title: GDH allostery and atomic model corrections.

Total number of manuscript pages: 35

Number of Tables: 3

Number of Figures: 8

ABSTRACT

Mammalian glutamate dehydrogenase (GDH) has complex allosteric regulation that is essential for a number of essential pathways¹. In particular, the loss of GTP inhibition causes the hyperinsulinism/hyperammonemia syndrome (HHS) where insulin is hypersecreted upon consumption of protein. The archetypical HHS lesion is H454Y and lies in the GTP binding pocket. To better understand the mechanism of HHS, we determined the crystal structure of this mutant. The mutation effects are limited to the H454Y GTP contacts. The bovine GDH crystal structures were then minimized to prepare for computational analysis and unusually large deviations were found near the allosteric NADH binding site. We found that this was due to the several errors in the older chemical sequence. Perhaps the error with the greatest impact on ligand binding was that residue 387 should be lysine rather than asparagine and is located in an allosteric site where activators (ADP and NAD⁺) and inhibitors (NADH, Epigallocatechin 3-gallate, and Epicatechin gallate) bind. All structures were re-refined and the electron densities for the bound ligands were greatly improved. The binding free energy differences for NADH binding were calculated using free energy perturbation to change lysine to asparagine at residue 387. The binding free energy penalty going from the correct to incorrect sequence found is +5 kcal/mol per NADH binding site. Additional analysis of this region of the protein suggests that the previous model for ADP activation is too simplistic. Therefore, correcting this error is important in understanding allostery and the development of GDH targeted therapeutics.

Keywords: Glutamate dehydrogenase, insulin, allostery, binding free energy

Broader Audience Abstract:

Glutamate dehydrogenase is a key enzyme involved in amino acid catabolism. As such, it is heavily regulated in animals by a wide array of metabolites. The importance of this regulation is most apparent in a genetic disorder called hyperinsulinism/hyperammonemia (HHS) where patients hypersecrete insulin upon the consumption of protein. We determined the atomic structure of one of these HHS mutants to better understand the disease and also analyzed the other major allosteric regulatory site.

INTRODUCTION

Mammalian glutamate dehydrogenase (GDH) is a homohexameric enzyme that catalyzes the reversible conversion of glutamate to α -ketoglutarate in the mitochondrial matrix². In animals, GDH is allosterically regulated by a wide range of small molecules with major activators being leucine and ADP and major inhibitors including GTP, NADH and palmitoyl CoA (for a review, see ¹).

While the existence of this complex allosteric regulation has been known for decades, the importance of GDH allostery has only been recently identified from studies on the Hyperinsulinism/Hyperammonemia Syndrome (HHS)^{3, 4}. HHS patients have point mutations that directly or indirectly abrogate GTP inhibition of GDH. Children with HHS have increased β -cell responsiveness to leucine and susceptibility to hypoglycemia following high protein meals⁵. This is likely due to uncontrolled amino acid catabolism that stimulates insulin secretion and yields high serum ammonium levels. In the pancreas, dysregulated GDH causes an exaggerated insulin response to amino acid consumption by increasing the flux of glutamate to α -ketoglutarate that, in turn, boosts ATP formation that stimulates insulin degranulation³. In the kidneys, high glutamate catabolism leads to increased ammonia output ⁶. In the CNS there is a high correlation between HHS and epilepsy, learning disabilities, and seizures that are independent of the high ammonium and hypoglycemia ⁷. This is likely because glutamate and its derivative, γ -aminobutyric acid, are important neurotransmitters.

The complexity of GDH allostery makes the thermodynamics and kinetics of GDH regulation in relation to its structure a long-standing problem ⁴. Since the bovine GDH protein sequence is 98% identical to human GDH sequence with 100% similarity near substrate and regulatory binding sites, bovine GDH is an excellent surrogate for human GDH.

GDH is a homohexamer composed of a dimer of trimers (Figure 3.1) ². Each monomer contains approximately 500 residues ². In the structure of the bovine GDH/NADH/Glu/GTP complex (Figure 3.1; pdb 3MW9), NADH and glutamate (the abortive complex) are observed in the active site and cause the ‘closed’ conformation where the NAD binding domain is closed tightly over the active site ². The inhibitor, GTP, binds at the base of the antenna between the pivot helix and the top of the NAD binding domain. A second molecule per subunit of NADH binds beneath the pivot helix between adjacent subunits and is presumed to inhibit GDH ⁸. This allosteric site is particularly complex since it binds the inhibitor ECG ⁹ as well as the activators ADP ¹⁰ and 75-E10 ¹¹.

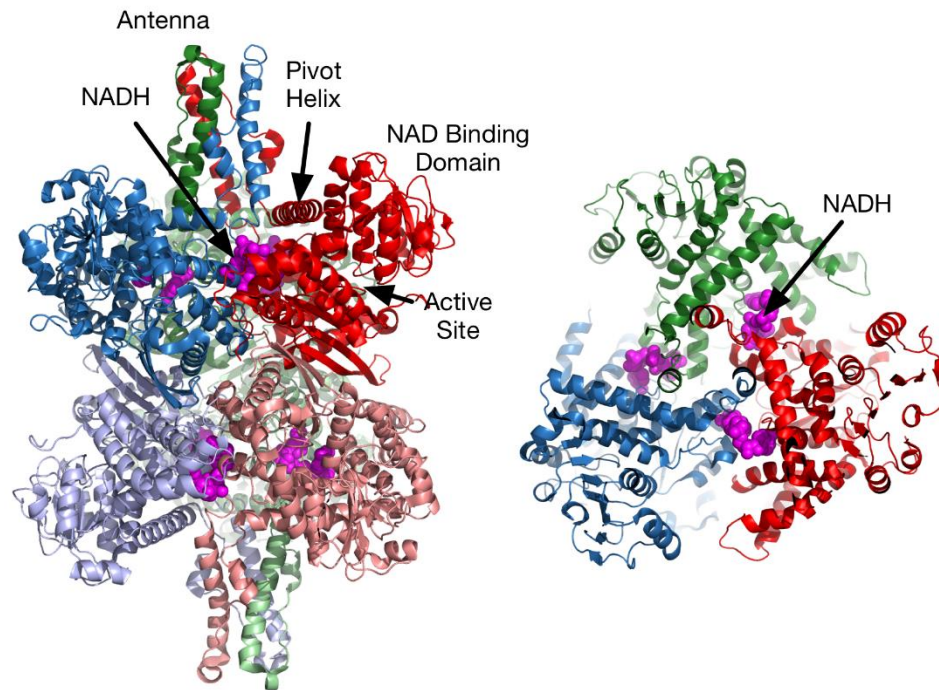


Figure 3.1: View of bovine GDH trimer in the inhibited state bound to NADH. NADH bound at the second site is shown in mauve. The trimer is composed of monomer A (blue), monomer B (red) and monomer C (green). The overlap of each NADH binding site between two adjacent monomers is shown.

The goal of this work was to examine the properties of the GTP inhibitory site with regard to HHS. We determined the structure of mutant human GDH with the HHS mutation, H454Y. Even though this mutation causes >400-fold decrease in sensitivity to GTP, it causes insignificant changes to the GTP binding site other than sterically interfering with GTP binding and eliminating a potential salt bridge with the β -phosphate. In other words, the conformation of the GTP binding site remains the same, but the presence of tyrosine eliminates favorable interactions GTP has with histidine. In preparation for *in-silico* studies on the GTP binding site, the structure of bovine GDH complexed with NADH/Glu/GTP was energy minimized. Abnormally high deviations from the starting structure were observed in the second, allosteric, NADH binding site. While trying to understand the cause for these deviations, we found several inconsistencies in the bovine GDH sequence that affects the x-ray crystallographic structures 1HWZ, 3MW9, 3MVQ, 1HWY, 1NQT, 1NR7, 3ETE, 3JCZ, 3MVO, 3QMU, 3ETD, 3ETG and the cryo-electron microscopy structures 3JCZ, 3JD0, 3JD1, 3JD2, 3JD3, 3JD4, 5K12^{2, 8-10, 12-15}. An interesting consequence of the errors involves the NADH/ADP/ECG allosteric binding site geometry and interactions. Further these sequence errors have nontrivial consequences on the computed thermodynamics of NADH binding and therefore other compounds at the same site. From the corrected and refined structures, it is also clear that the previously proposed model for ADP activation is likely too simplistic.

MATERIALS AND METHODS

Structure determination of the H454Y-huGDH mutant.

The H454Y mutant of human GDH was cloned, expressed, and purified as previously described¹⁶. H454Y GDH crystals were prepared using the vapor diffusion method and sitting drop apparatus. The enzyme was dialyzed against 0.1M sodium phosphate, pH 6.8 and adjusted to a concentration of 3.75mg/ml. The reservoir solution contained 10% PEG 8000 (w/v), 0.1M sodium chloride, 1.3% octyl- β -glucopyranoside (w/v), 7.5% methyl pentanediol (v/v), 0.1M sodium phosphate, pH 6.8, and 1mM sodium azide. The drop was composed of 8 μ l reservoir, 1.35 μ l enzyme solution, and 0.65 μ l water. The crystals were prepared for freezing in the Oxford system cryostream by incubation in a synthetic mother liquor solution containing increasing concentrations of glycerol. This solution contained 60mM sodium phosphate, 1% octyl- β -glucopyranoside (w/v), 8% methylpentanediol (v/v), 50mM sodium chloride, 14% PEG 8000 (w/v), and 1mM sodium azide. The crystals were incubated for 30 minutes in this solution containing 0, 2, 5, and 10% glycerol (v/v). At the end of these incubations, the concentration of PEG 8000 in the synthetic mother liquor was increased to 22%, and the crystals were incubated for 30 minutes in each of the solutions containing 12.5, 15, 17.5, and 20% glycerol. Data was collected from a single crystal with dimensions of 0.22mm x 0.24mm x 0.11mm on a R-axis IV imaging plate system attached to a Rigaku generator. The data set is composed of 260 diffraction images with oscillation angles of 0.4° and exposure times of 45 min. The crystal belonged to the space group P1 and had unit cell parameters of $a=96.78\text{\AA}$, $b=98.44\text{\AA}$, $c=124.28\text{\AA}$, $\alpha=85.95$, $\beta=69.34$, and $\gamma=60.98$. The data collection statistics are shown in Table 3.1.

Since this unit cell was nearly identical to that of the previously characterized native huGDH crystals ¹⁷, molecular replacement was used to determine this structure. Phenix and COOT were used for structure determination and refinement, respectively. Initially, the model was subjected to thirty steps of rigid body refinement without non-crystallographic (NCS) restraints and then energy minimization with NCS restraints to make sure the coenzyme binding domain was free to move if necessary. Simulated annealing was then applied with NCS restraints, followed by energy minimization and individual B value refinement. The histidine at position 454 (mutation site) was initially modeled as an alanine. After two rounds of crystallographic refinement, a tyrosine residue was modeled with respect to the electron density observed in a $2F_o-F_c$ map. This was further corroborated by analysis of a F_o-F_c map with both positive and negative contours. The final refinement statistics are summarized in Table 3.1(b).

Sequence Analysis

Bovine and human GDH share 100% sequence identity in the allosteric binding sites. Thus, when residue 387 was found by modeling comparison to be identified as asparagine in bovine but lysine in human, the bovine GDH sequence was reinvestigated ¹⁸. ¹⁹. The bovine GDH sequence originally used in all bovine GDH structures came from a protein sequence determined by chemical modification published in 1972¹⁵ Five residues were misidentified: N387K, G47S, A248V, V271I and A272T. Of the five, only N387K was located in a binding site and was determined to be the most deleterious to previous interpretations of function.

Model Refinement

Crystal structure 3MW9 containing the incorrect sequence was minimized by conjugate gradient for 4000 steps using the NAMD software. The root-mean-square deviation was calculated for each atom using the incorrect sequence crystal structure as the

reference state. A number of atoms located near the allosteric ligand binding pocket moved greater than 3Å which is unusual for a 2.7Å structure. We compared the NADH binding pocket (Figure 1) of 3MW9 (incorrect sequence) to a crystal structure of H454Y mutant human GDH. When comparing both structures, it was evident that the sequences near the NADH allosteric site were not identical when considering the free phosphate molecules located near the NADH binding pocket in the mutant human GDH structure, which should be in a similar location as the NADH β -phosphate group in 3MW9 (incorrect sequence). Thus, residues located near the NADH binding pocket, particularly those near the NADH phosphate group, were further analyzed via sequence alignment.

Free Energy Simulation

As we are interested in ligand binding to the allosteric sites, we calculated the consequences of the sequence/structure issue on binding free energy differences in the presence and absence of NADH. The GDH model used for simulation was the homotrimer (see Figure 1). We considered the difference in unbound vs NADH bound to pdb 3MW9 in the previously published form and with the correct sequence. Each pair of monomers contained a NADH molecule bound to the NADH binding site (3 NADH molecules bound total) and each monomer initially contained the correct residue (Lys 387). This structure was placed in 0.1M NaCl solution, minimized for 6000 steps and equilibrated for 1ns in an NPT ensemble with a 2 fs time step. The CHARMM36 force field was used for atomic topology and parameters. Particle-mesh Ewald with tinfoil boundary conditions was used for the long range electrostatic calculations. The free energy was then computed for changing Lys to Asn at residue 387. The dual topology technique was used to calculate the binding free energy, where $\lambda=0$ state is Lys 387 and $\lambda=1$ state is Asn 387. The binding free energy simulations were run for over 100 nanoseconds per λ . The calculation was divided into 16 windows and the free energy was calculated using free energy perturbation techniques

(Equation 1), where k_B is the Boltzmann constant, T is the temperature at 300K and $\langle \rangle$ represents the ensemble average ²⁰.

$$\Delta G = -k_B T \ln \langle e^{-\beta \Delta U} \rangle \quad (1)$$

The binding free energy difference ($\Delta\Delta G$) was calculated for the thermodynamic cycle shown in Figure 2.1. $\Delta\Delta G$ may be computed as the difference of the vertical legs, which is equal to the difference of the horizontal legs. The horizontal legs of the thermodynamic cycle (ΔG_1 and ΔG_3) represents the free energy of changing lysine to asparagine with and without NADH. ΔG_1 and ΔG_3 are the sums of their electrostatic terms and van der Waals terms.

RESULTS

Structure of the H454Y mutant

Several mutations in the GTP binding site and antenna desensitizes GDH to GTP inhibition^{21, 22}. While the HHS H454Y mutant has been extensively studied and is used as an archetypal example of HHS^{16, 23}, the structural effects of the mutation had not been determined. The structure of H454Y was determined to 2.7Å (Table 3.1, Figure 3.2). Using the alignment routine in Pymol²⁴, the structure of apo human GDH was compared to apo H454Y human GDH and the root-mean-square difference between the two structures was 0.35Å (using 2855/3872 atoms). As with all apo GDH structures, the outermost region of the NAD⁺ binding domain has weak density because of its inherent flexibility in the absence of bound substrates. However, the electron density around the GTP site was well resolved and clearly showed the H454Y mutation (Figure 3.2A). As shown in Figure 3.2B, the H454Y mutation does not affect any of the neighboring residues. Therefore, it is most likely that the H454Y mutation directly interferes with GTP binding rather than by deforming the binding site. To better examine this, the H454Y mutation was modeled in the bovine GDH structure (H450Y in bovine GDH) where we have the structure of GTP bound. Since the huGDH H454Y structure demonstrated that the mutation does not affect other residues in the GTP binding site, we made the H450Y mutation in bovine GDH using the VMD plug-in, Mutator. The complex placed in 0.1M NaCl and GDH was held fixed while the solvent was minimized for 2,000 steps. The solvent was then held fixed and GDH and its ligands were minimized for 200 steps. The entire system was then minimized for 2000 steps. As shown in Figure 3.2C, the effects of the tyrosine at 450 appear to be modest. The hydroxyl group is very close to the β -phosphate of the GTP and may sterically interfere with the phosphate interactions. Perhaps more importantly, the His to Tyr mutation would likely eliminate the charge interaction.

Wavelength	
Resolution range	29.77-2.7 (2.797-2.7)
Space group	P1
Unit cell (a,b,c,α,β,γ)	96.803, 98.38, 124.3, 85.94, 69.35, 61.0
Unique reflections	90899 (7177)
Multiplicity	2.2(2.0)
Completeness (%)	88.82 (70.29)
Mean I/sigma(I)	12.9 (2.0)
Wilson B-factor	45.77
R-merge	0.06 (0.24)
Reflections used in refinement	90875 (7176)
Reflections used for R-free	4607 (362)
R-work	0.2406 (0.2898)
R-free	0.2786 (0.3737)
Number of non-hydrogen atoms	23591
macromolecules	23256
ligands	75
solvent	260
Protein residues	2976
RMS(bonds)	0.008
RMS(angles)	0.95
Ramachandran favored (%)	91.36
Ramachandran allowed (%)	6.88
Ramachandran outliers (%)	1.75
Rotamer outliers (%)	5.73
Clashscore	10.71
Average B-factor	61.78
macromolecules	61.95
ligands	66.92
solvent	45.24

Table 3.1. Data collection and refinement statistics. Statistics for the highest-resolution shell are shown in parentheses. $R_{\text{merge}} = \sum_{hkl} (\sum_i (|I_{hkl,i} - \langle I_{hkl} \rangle|)) / \sum_{hkl} \sum_i I_{hkl,i}^*$

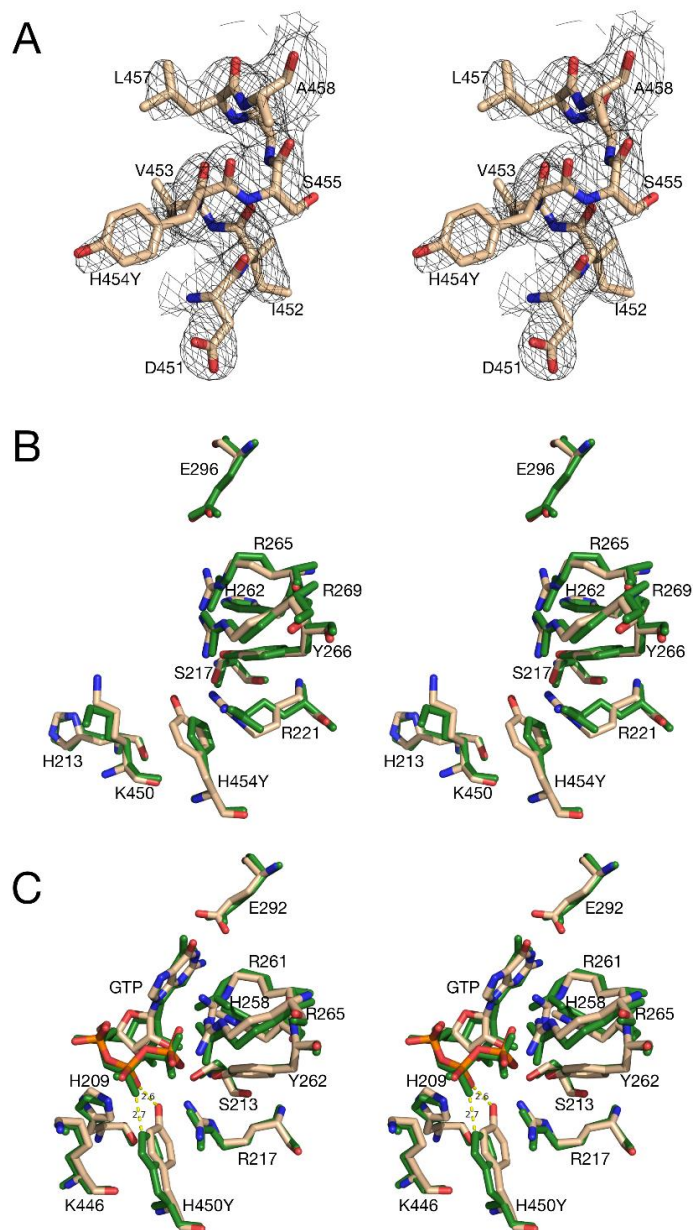


Figure 3.2: Structure of the HHS H454Y mutant. A) Shown here is the electron density of the region around the human GDH H454Y mutation that causes HHS. B) This figure shows the structures of the sidechains that contact GTP before (green) and after the mutation. C) Shown here are the energy minimized structures of bovine GDH complexed with GTP/NADH/Glu before (green) and after the H450Y (H454Y in human) mutation.

Electron Density versus Protein Sequence

In preparation for examining GDH allostery, we compared the wild type crystal structure to its minimized structure and searched for residues that moved more than 3Å away from their initial position. This was done to see if there were any significant deviations in the GDH allosteric ligand binding pockets. The atoms in the GTP binding site remained well within 3Å of their respective crystal position while atoms in the NADH binding site deviated greater than 3Å. This led to the further investigation of residues in the NADH binding site.

To ensure consistency of the NADH binding pocket between the H454Y mutant GDH and the wild type GDH, both the residue composition and conformation were compared. It was found that residue 387 was a lysine in the H454Y mutant structure and asparagine in the bovine GDH structure. As mentioned earlier, there should be a 100% identity between the bovine and human GDH sequences near the NADH binding site. However, the older published bovine GDH sequence had residue 387 incorrectly identified as asparagine instead of lysine which was used in the crystal structure refinements. Residue 387 is located at the interface of the allosteric NADH binding site. Table 3.1 shows the distances between residue 387 and NADH in the incorrect, correct and mutant GDH crystal structures. As shown in Table 3.2, the distance between NADH and residue 387 is reduced by 63% when correcting residue 387 from an asparagine to a lysine. This moves the NADH β -phosphate one shell (water diameter) closer to the NADH binding site, which is similar to the free PO_4^{3-} ligand in the H454Y mutant NADH binding site. This geometric difference affects the binding free energy of NADH interacting with residue 387. Thus, we calculated the binding free energy difference of lysine versus asparagine in the presence and absence of NADH to compute the significance of the N387K sequence error for future drug or ligand design.

GDH Complex	Ligand	387 to Ligand Distance (Å)
Incorrect bovine seq (N387)	NADH(βPO_4^{3-} group)	6.2
Correct bovine seq (K387)	NADH (βPO_4^{3-} group)	3.9
H454Y Mutant human GDH	PO_4^{3-}	3.2

Table 3.2: Distances (Å) between residue 387 and ligand in NADH binding pocket in the incorrect bovine GDH, correct bovine GDH, and H454Y mutant human GDH.

Evidence for the sequence error in the electron density

Shown in Figure 3.3 is the difference map ($F_o - F_c$) when 387 is an asparagine and the $2F_o - F_c$ map after it was substituted by a lysine and re-refined. In the difference map, the red density represents negative density where atoms should not be in the model while the positive blue density shows areas lacking atoms in the model. After refinement, the $2F_o - F_c$ density well describes the lysine sidechain. Thus, the crystallographic data had pointed to, and been consistent with, the error in the published sequence.

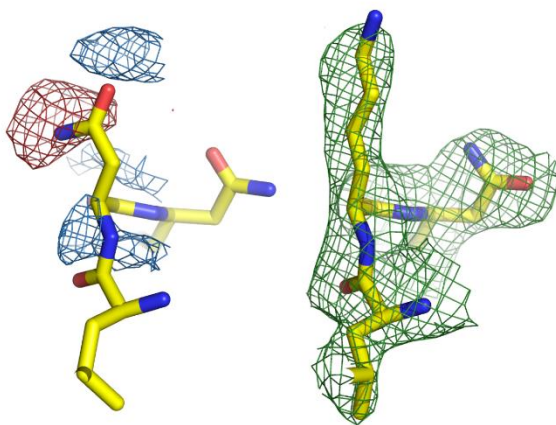


Figure 3.3: Comparison of asparagine and lysine in 3MW9 electron density at residue 387. Asparagine (left) in the electron density is unfavorable as indicated by the negative and positive electron density, (red and blue respectively) in the Fo-Fc maps. However, these differences disappear when lysine is used instead. It is important to note that the position of asparagine and lysine are different in the figure because the re-refinement of 3MW9 resulted in a conformational change when using lysine instead of asparagine in the protein sequence.

Computed Free Energy Penalty

The total computed binding free energy penalty is +5 kcal/mol per NADH between the incorrect and correct sequence forms. This was an average from all three binding sites. (Figure 3.4). The errors were calculated using the block standard error (BSE) method²⁵ with a block size of 1000. The maximum errors in any window (see eq 1) for ΔG_1 electrostatics, ΔG_1 van der Waals, ΔG_3 electrostatics, and ΔG_3 van der Waals were ± 0.086 kcal/mol, ± 0.043 kcal/mol, ± 0.047 kcal/mol and ± 0.046 kcal/mol, respectively. The standard square root of the sum of each window's variance for ΔG_1 electrostatics, ΔG_1 van der Waals, ΔG_3 electrostatics, and ΔG_3 van der Waals were ± 0.20 kcal/mol, ± 0.088 kcal/mol, ± 0.13 kcal/mol and ± 0.11 kcal/mol, respectively. We can use a more conservative propagation of errors taken as the sum of the 16 window errors, shown in Table 3.3.

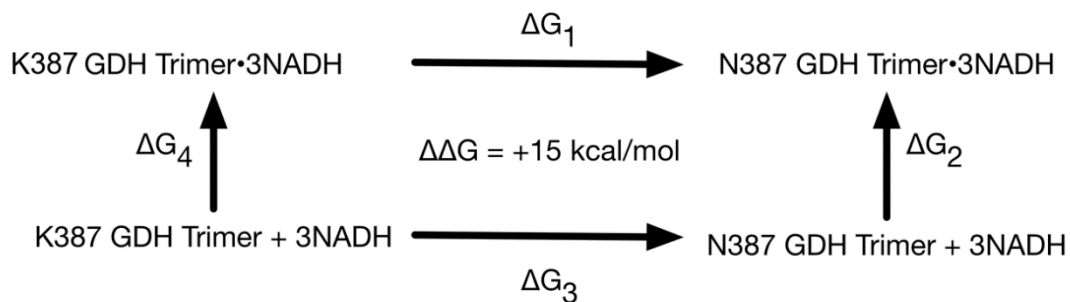


Figure 3.4: Thermodynamic cycle used to calculate the binding free energy difference of asparagine versus lysine as residue 387.

$\Delta G_1 = 107 \pm 1.1$	$\Delta G_3 = 92 \pm 0.94$
$\Delta G_1 \text{ electrostatics} = 99 \pm 0.77$	$\Delta G_3 \text{ electrostatics} = 83 \pm 0.52$
$\Delta G_1 \text{ van der Waals} = 8 \pm 0.36$	$\Delta G_3 \text{ van der Waals} = 9 \pm 0.42$

Table 3.3: Binding Free Energy differences in kcal/mol for the trimer with summed window errors using BSE n=1000.

The size of the computed sequence error effect on the free energy of binding for the native ligand, NADH, would preclude any productive sort of computational screening of other compounds based on free energy calculations with such a structure.

Structural analysis of the NADH/ADP/ECG site

As mentioned above, the NADH allosteric site is particularly puzzling since it binds both activators (ADP) and inhibitors (NADH and ECG/EGCG). While we have not yet determined the structure of GDH complexed with the compound 75-E10, our previous binding studies demonstrated that it likely binds to this same site as well ¹¹. Shown in Figure 3.5 is the electron density of bound NADH, ADP, and ECG bound to this site. In all cases, the quality of the electron density improved upon re-refining these complexes with the corrected sequence. With the change of N387 to K387, it is necessary to reexamine the interactions between GDH and the various allosteric regulators that bind to this site to better understand how the various ligands can cause such disparate effects (Figure 3.6). The view in this figure is approximately parallel to the ‘pivot helix’, looking into the interface between two subunits within one of the trimers. To emphasize that this allosteric site is at the interface between two adjacent subunits, the carbon atoms in the stick models are shown in light blue or white. Each of the figures is labeled as either being ‘open’ or ‘closed’ to denote the conformation of the catalytic cleft. It is immediately evident that the

newly introduced K387 interacts with all three ligands in both the open and closed conformations while the previous erroneous N387 did not.

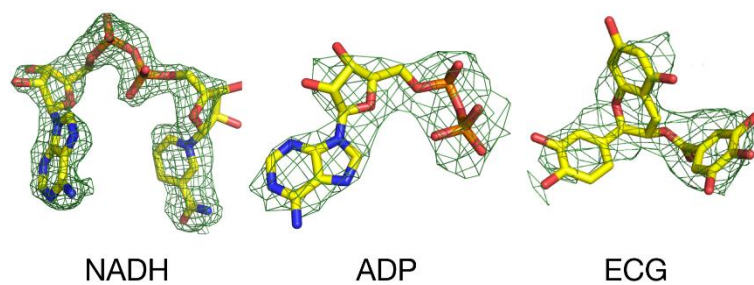


Figure 3.5: Electron density for the re-refined ligands bound to the NADH/ADP/ECG site.

Also noted on the figures are the results of our previous site-directed mutagenesis studies ⁹. In the case of ADP, R86S and S393I mutations had deleterious effects on activation. The R86S mutation effects are not entirely surprising since the guanidine group on the arginine stacks up against the purine ring in addition to interacting with the ribose hydroxyl groups. The effects of the S393I mutation are more complex in that S393 interacts with all of the bound ligands but the mutation also abrogates GTP inhibition even though it does not contact GTP. Therefore, it is not clear whether the S393I effects are entirely due to changes in the binding interface or whether it may also be related to subunit/subunit communication as implied by the loss of ADP and GTP regulation when the antenna is genetically removed ²⁶. R459 interacts extensively with the β -phosphate of ADP. When mutated to an alanine, ADP activation is completely abrogated. However, using TNP-ADP as a fluorescent ADP analog ²⁶, it was clear that the R459A mutation did not block ADP binding. This was somewhat unexpected and suggested that the mutation did not affect binding but rather the conformational changes necessary for ADP activation. The existence of this unusual phenomenon was also suggested by the fact that the R459A mutation increased the ED₅₀ for diethylstilbestrol (DES) and GTP by nearly 5-fold and palmitoyl-CoA by approximate 3-fold. From the structure of DES, it is likely to bind to the GW5074/bithionol site deep within the enzyme rather than the ADP site¹³. Therefore, the effects of the R459A mutation is not simply removing a charge on the pivot helix that interacts with ADP. The effects of the D119A mutation is more simply understood. As shown in this figure, the carboxylic acid group of D119 is close to the β -phosphate of ADP and the charge on this acid is at least partially negated by the basic residues in the area. Unlike the other mutations, the D119A mutant enhances the activation of ADP by approximately 2-fold. It seems most likely that this mutation enhances binding and/or action by increasing the positive charge in that area.

The effects of NADH bound to this site is less clear. NADH inhibition is only seen at very high NADH concentrations, well above the measured binding of NADH to this

site¹. Nevertheless, it is well documented that GTP and NADH bind in a synergistic manner²⁷ and this structure is in the ‘closed’ conformation where the catalytic mouth is closed tightly on the abortive complex of NADH+Glutamate². Two of the more notable changes are the positions of H209 and R459. In the open conformations in the ECG and ADP structures, both of these residues are rotated down onto the bound ligand. Here, H209 rotates and interacts with the bound GTP while R459 is lifted up and away from the NADH because of the closed conformation. The adenosine/ribose rings of the bound NADH closely mimic that of ADP. However, the nicotinamide/ribose moiety hooks back down into the protein near the base of the antenna. It is not clear whether this nicotinamide/ribose moiety binding here causes inhibition and why NADH inhibition requires such a high concentration relative to its K_d.

The structure of ECG is similar to ADP in that it is bound to the open conformation of GDH in spite of the fact that NADPH was added to the crystallization mixture⁹. In this conformation, H209 swings over to interact with the gallate ring (ring D) but does not interact to the extent that the α -phosphate does in the ADP structure. Also, similar to ADP, R459 swings down from the pivot helix to interact with the gallate ring. While the D119A mutation enhances ADP activation, the same mutation abrogates ECG inhibition. The difference is likely due to the fact that the carboxyl side chain forms hydrogen bonds with the C ring of the flavanol moiety that are lost with the D119A mutation while the negation of these charges eliminates the charge conflict around the β -phosphate in ADP. As with ADP, the R86S mutation blocks ECG inhibition presumably by eliminating a hydrogen bond to the OAR atom of the C ring of the flavanol group.

The N387K fixed and refined structures all yield more accurate details of the ligand/GDH contacts. However, it is still puzzling why some ligands binding to this site activate while others inhibit the enzyme. As we noted previously, GDH is a highly flexible enzyme that undergoes large conformational changes during each catalytic cycle¹. To better quantify these structural changes, several measurements were made comparing the

open (ADP/GDH) and closed (GTP/NADH/GLU/GDH) structures (Figure 3.7). To better illustrate the movements described below, the ascending antenna helices (red helix) of the open (lighter hues) and closed (darker hues) conformations were aligned in this figure (noted as #1). In the first measurement, the center of masses of the pivot helices were calculated and found to move $\sim 2.5\text{\AA}$ away from each other as the catalytic site closes (#3 and #4). Similarly, when the bottom quarter (N-terminal end) of the ascending helices were analyzed, they also moved $\sim 2.5\text{\AA}$ away from each other as the catalytic site closes. However, the distances between the top quarter of the ascending helices remained unchanged as the catalytic site closed. Essentially, that portion of the three helices (#5) is the pivot point about which the ascending helices rotate about each other as the catalytic site opens and closes. The descending helix of the antenna (#6) is caught right in the middle of this conformational change with the top (N-terminus) being fixed near the pivot axis and the bottom (C-terminus) being carried along for the 2.5\AA expansion as the catalytic site closes. For this reason, the helix itself is distended in the closed conformation.

From these results, the effects of the various activators and inhibitors binding to this same site maybe be due to more than particular GDH/ligand interactions but rather due to the large conformational changes occurring in this subunit interface. For example, one of the HHS mutations that abrogates GTP inhibition lies in this helix ¹⁷ and the deletion of the antenna region eliminates both GTP and ADP regulation ²⁶. The S393I mutation not only affects ADP activation but GTP inhibition as well. From these and several other observations, it is apparent that the widely varying effects of ADP, NAD^+ , ECG, and 75-E10 binding to this site may not be due to interactions with particular residues but rather their larger effects on this complex movement between adjacent subunits within the trimers.

The schematic in Figure 3.7B summarizes these movements in entire hexamer. When the substrate binds (#1), the NAD binding domain rotates by $\sim 20^\circ$ about the pivot helix (#2) and tightly closes the catalytic cleft (mouth). The base of the antenna rotates

away from that subunit (#3) and pushes into the NAD binding domain of the adjacent subunit. In this side view of the adjacent subunit, closure of the catalytic cleft from #2 rotates the NAD binding domain away from the center of the hexamer (#4). This, in turn, opens up the ADP binding site (#5). All of these rotations and twisting motions compresses the core of the hexamer (#6).

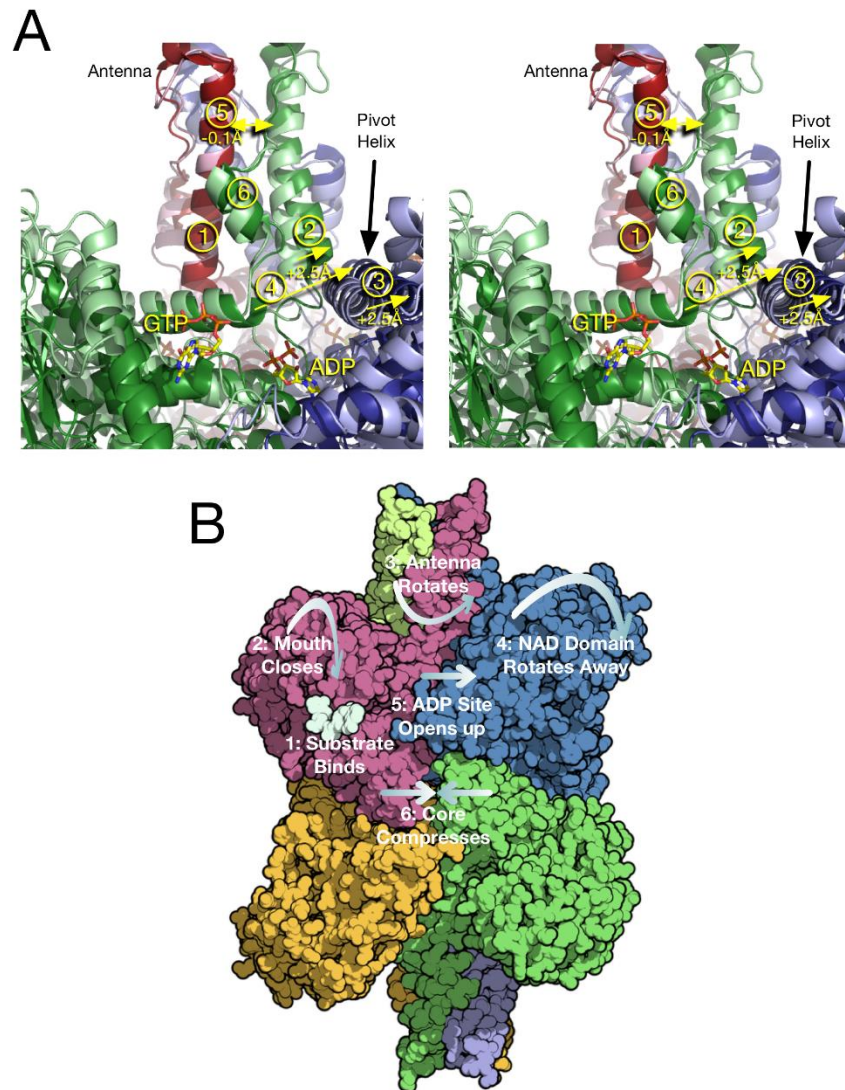


Figure 3.7: A) Expansion and contraction of the NADH/ADP/ECG binding site. GDH trimers from the open mouth (lighter hues) and closed mouth (darker hues) are aligned along one of the ascending antenna helices (#1). As the catalytic mouth closes, the ascending antenna helices (#2) and the pivot helices move $\sim 2.5\text{\AA}$ away from each other (#3, #4) causing an opening of the NADH/ADP/ECG binding site. This rotation occurs about the upper quarter of the ascending antenna helices (#5), causing a distension of the descending antenna pivot helix (#6). B) Schematic of the overall movement in GDH as the catalytic mouth closes. GDH binds (#1) causing the NAD binding domain to rotate and close upon the substrate (#2). The base of the antenna rotates counter clockwise (#4) and the NAD binding domain rotates away from the center of the hexamer. These rotations are twisting motions that cause the core of the hexamer to compress (#5).

To better visualize the effects of these rotations and movements on the ADP binding site, Figure 3.8 shows a surface rendering of this binding site in the open and closed conformations. As with Figure 3.7A, the open conformation is represented by lighter hues and the two adjacent subunits are colored in green and blue. The view here is approximately parallel to the antenna, looking down into the allosteric site. In general, as the catalytic site closes, the gap between the two subunits expand, enlarging the binding pocket. In the case of the NADH/GLU/GTP/GDH complex, this allows for the nicotinamide/ribose moiety of NADH to penetrate further into the subunit interface. Interestingly, this could explain the binding synergy between GTP and NADH²⁸. Our previous structural analysis showed that the triphosphate binding site for GTP only opens up when the catalytic site is closed. Here, it seems that NADH would also prefer the closed conformation by virtue of the enlarged binding pocket. Therefore, it seems likely that the positive binding cooperativity between these two ligands²⁸ is due to this selection of the closed conformation. As the catalytic site opens, this binding cavity compresses and the pivot helix rotates back towards it. This places R459 directly above it and makes a smaller binding pocket that is better suited to the ADP structure. An overly simplistic interpretation of this effect in relationship to ADP activation is that the binding of ADP helps to compress this allosteric site that in turn makes it easier to open the catalytic cleft and release the product. However, the ECG complex appears to argue against this simple model. ECG was found to bind to the open

conformation in spite of the addition of NADPH to the crystallization mixture. Therefore, ligands that prefer the smaller pocket found in the open conformation are not necessarily all activators.

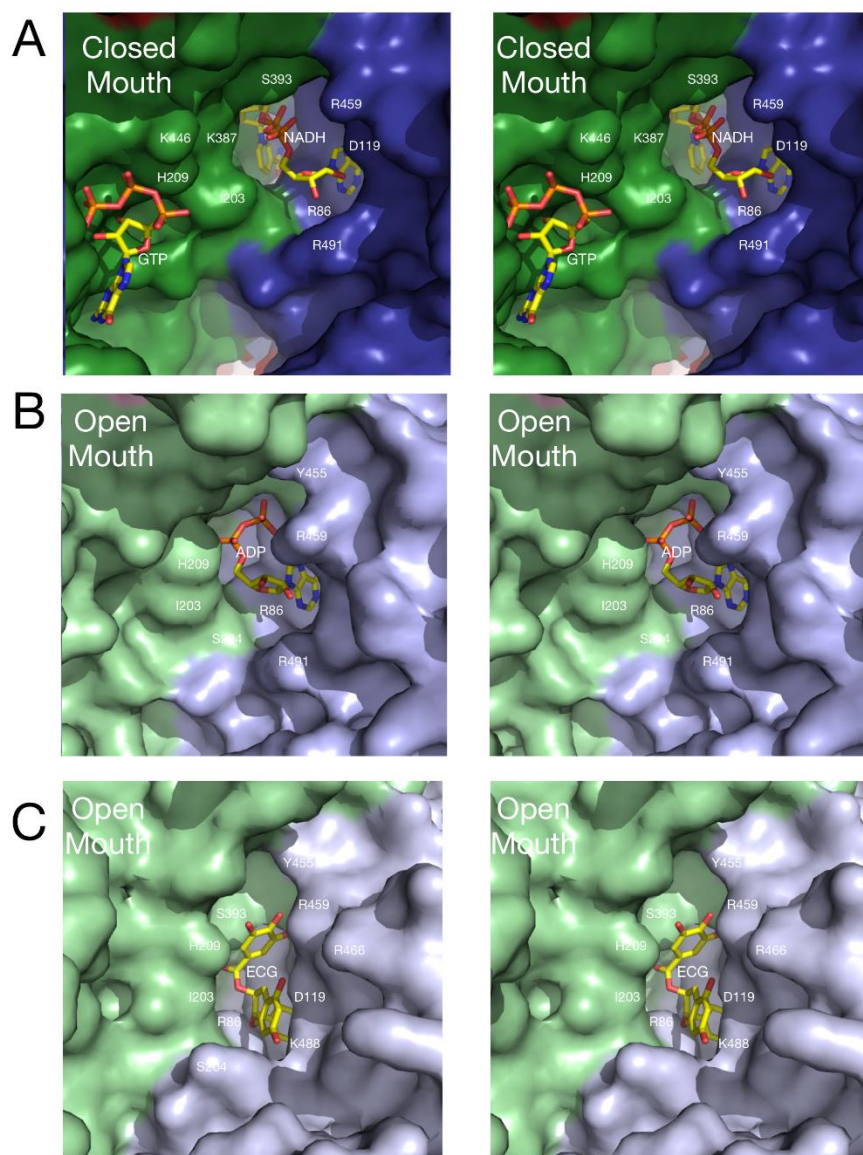


Figure 3.8: Surface details of the NADH/ADP/ECG binding site. In the closed mouth conformation, the subunits (green and blue) spread apart by 2.5\AA , making more room for the bound NADH in the top figure. In contrast, the subunits compress by 2.5\AA in the open mouth conformation, making for better interactions with the smaller allosteric ligands.

DISCUSSION AND CONCLUSIONS

The original published sequence of bovine GDH has been used for a large number of studies^{2, 8-10, 12-15} but unfortunately contained a few mistakes including that at residue 387¹⁸. Those studies included 18 x-ray diffraction and cryo-electron microscopy structures^{2, 8-10, 12-15}. Lysine is the correct amino acid identity of residue 387 in the allosteric NADH binding site, not asparagine. The thermodynamic impact of this mistake is shown to be +5 kcal/mol per NADH binding site which would disrupt most modeling and virtual screening studies for allosteric compounds. In addition to residue 387, four other residues were corrected in the bovine GDH sequence, specifically G47S, A248V, V271I and A272T. However, unlike N387K, these residues were located far from allosteric and catalytic binding sites and are unlikely to require significant changes in interpretations.

The adjusted structures were re-refined with particular attention being paid to the ligands bound to this allosteric site. Notably, the quality of the density for NADH, ADP, and ECG all improved with N387K adjustment. However, as before, the density for the outermost regions of the NAD binding domain were very poor in the open conformation compared to that of the closed structure (GTP/NADH/GLU/GDH) even when the positions of all 12 NAD binding domains were refined individually. This strongly suggests that the NAD binding domain has marked flexibility when not clamped down upon substrate.

Together, these results suggest a modification of our previous model for GDH allostery¹⁰. Whereas emphasis was placed on the rotation of the pivot helix and the interactions between R459 and the β -phosphate of ADP, it now seems more likely that allostery at this site depends upon the expansion and contraction between subunits within the trimer as the catalytic site closes and opens, respectively. Since this motion involves a wide area of the enzyme, including the entire antenna, there are numerous sites where allosteric ligands and mutations could affect catalysis. Further, it becomes less of a paradox

as to how different ligands can bind to the same location and cause opposite effects since this expansion/compression process is such a large system of conformational changes.

Previous biochemical data on the H454Y mutant also suggests that allosteric regulation of GDH is more complex than just ligands binding to their corresponding sites¹⁶. The K_i for GTP in wild type human GDH is ~40nM and this increases by ~400-fold (16μM) with the H454Y mutation. Interestingly, when the GDH from lymphoblasts was examined from patients with the H454Y lesion, the inhibition pattern was monophasic with a K_i for GTP of ~250nM. The monophasic nature of the inhibition curve suggests that the GDH in the patients is a chimeric mix of the two types of subunits. If both types of subunits are approximately equally expressed in the patients, then it follows that the effects of the H454Y mutant are greatly dampened by having even a fraction of wild type subunits. This would be consistent with the implications outlined above where subunit communication plays a major role in the effects of allosteric regulators. In this case, the apparent cooperativity among the wild type subunits is sufficient to overcome the lack of GTP binding to the H454Y subunits. Importantly, this is in agreement with our previous finding that eliminating the antenna, that does not bind any of the allosteric effectors, eliminates ADP, GTP, and ECG regulation²⁶. Clearly, further studies are necessary to fully understand the structural details of the structural changes that occur in the hexamer after allosteric ligand binding.

REFERENCES

1. Smith HQ, Li C, Stanley CA, Smith TJ. Glutamate dehydrogenase; a complex enzyme at a crucial metabolic branch point. *Neurochemical Res.* 2017.
2. Peterson PE, Smith TJ. The structure of bovine glutamate dehydrogenase provides insights into the mechanism of allostery. *Structure Fold Des.* 1999;7:769-782.
3. Stanley CA, Lieu YK, Hsu BY, et al. Hyperinsulinism and hyperammonemia in infants with regulatory mutations of the glutamate dehydrogenase gene. *New England Journal of Medicine.* 1998;338:1352-1357.
4. Smith TJ, Stanley CA. Untangling the glutamate dehydrogenase allosteric nightmare. *Trends in Biological Chemistry.* 2008;33:557-564.
5. Hsu BY, Kelly A, Thornton PS, Greenberg CR, Dilling LA, Stanley CA. Protein-sensitive and fasting hypoglycemia in children with the hyperinsulinism/hyperammonemia syndrome. *J Pediatr.* 2001;138:383-389.
6. Treberg JR, Clow KA, Greene KA, Brosnan ME, Brosnan JT. Systemic activation of glutamate dehydrogenase increases renal ammoniogenesis: implications for the hyperinsulinism/hyperammonemia syndrome. *Am J Physiol Endocrinol Metab.* 2010;298:E1219–E1225.
7. Bahi-Buisson N, Roze E, Dionisi C, et al. Neurological aspects of hyperinsulinism-hyperammonemia syndrome. *Dev. Med. & Child Neurol.* 2008;50:945-949.
8. Smith TJ, Peterson PE, Schmidt T, Fang J, Stanley C. Structures of bovine glutamate dehydrogenase complexes elucidate the mechanism of purine regulation. *J. Mol. Biol.* 2001;307:707-720.
9. Li C, Li M, Narayan S, et al. Green tea polyphenols control dysregulated glutamate dehydrogenase in transgenic mice by hijacking the ADP activation site. *J. Biol. Chem.* 2011;286:34164-34174.
10. Banerjee S, Schmidt T, Fang J, Stanley CA, Smith TJ. Structural studies on ADP activation of mammalian glutamate dehydrogenase and the evolution of regulation. *Biochemistry.* 2003;42:3446-3456.
11. Smith HQ, Smith TJ. Identification of a Novel Activator of Mammalian Glutamate Dehydrogenase. *Biochemistry.* 2016;55:6568–6576.
12. Bailey J, Powell L, Sinanan L, et al. A novel mechanism of V type zinc inhibition of glutamate dehydrogenase results from disruption of subunit interactions necessary for efficient catalysis. *FEBS.* 2011;278:3140-3151.

13. Li M, Smith CJ, Walker MT, Smith TJ. Novel inhibitors complexed with glutamate dehydrogenase: allosteric regulation by control of protein dynamics. *J. Biol. Chem.* 2009;284:22988-23000.
14. Merk A, Bartesaghi A, Banerjee S, et al. Breaking Cryo-EM Resolution Barriers to Facilitate Drug Discovery. *Cell.* 2016;165:1698-1707.
15. Borgnia MJ, Banerjee S, Merk A, et al. Using Cryo-EM to Map Small Ligands on Dynamic Metabolic Enzymes: Studies with Glutamate Dehydrogenase. *Molecular Pharmacology.* 2016;89:645-651.
16. Fang J, Macmullen C, Smith TJ, Stanley CA. Expression, purification, and characterization of human glutamate dehydrogenase (GDH) regulatory mutations associated with a dominantly-expressed congenital hyperinsulinism / hyperammonemia syndrome. *Biochem. J.* 2002;363:81-87.
17. Smith TJ, Schmidt T, Fang J, Wu J, Siuzdak G, Stanley CA. The structure of apo human glutamate dehydrogenase details subunit communication and allostery. *J. Mol. Biol.* 2002;318:765-777.
18. Moon K, Piszkiwicz D, Smith EL. Glutamate dehydrogenase: amino acid sequence of the bovine enzyme and comparison with that from chicken liver. *Proc. Natl. Acad. Sci. U.S.A.* 1972;69:1380-1383.
19. Michaelidis TM, Tzimagiorgis G, Moschonas NK, Papamatheakis J. The human glutamate dehydrogenase gene family: gene organization and structural characterization. *Genomics.* 1993;16:150-160.
20. Zwanzig RW. High-temperature equation of state by a perturbation method. I. Nonpolar gases. . *J. Chem. Phys.* 1954;22:1420-1426.
21. Hsu BYL, Kharlip J, Fang J, Poncz M, Glaser B, Stanley CA. "Leucine Sensitive Hypoglycemia" caused by dominantly-inherited mutations of glutamate dehydrogenase. *Pediatr Res.* 1998;43:78A (SPR meeting abstract).
22. MacMullen C, Fang J, Hsu BYL, et al. Hyperinsulinism/hyperammonemia syndrome in children with regulatory mutations in the inhibitory guanosine triphosphate-binding domain of glutamate dehydrogenase. *J Clin Endocrinol Metab.* 2001;86:1782-1787.
23. Li C, Allen A, Kwagh K, et al. Green Tea Polyphenols Modulate Insulin Secretion by Inhibiting Glutamate Dehydrogenase. . *J. Biol. Chem.* 2006;281:10214-10221.
24. DeLano WL. The PyMOL Molecular Graphics System. . Palo Alto, CA, USA: DeLano Scientific LLC; 2008.

25. Grossfield A, Zuckerman DM. Quantifying uncertainty and sampling quality in biomolecular simulations. *Annual reports in computational chemistry*. 2009;5:23-48.
26. Allen A, Kwagh J, Fang J, Stanley CA, Smith TJ. Evolution of glutamate dehydrogenase regulation of insulin homeostasis is an example of molecular exaptation. *Biochemistry*. 2004;43:14431-14443.
27. Dieter H, Koberstein R, Sund H. Studies of glutamate dehydrogenase. The interaction of ADP, GTP, and NADPH in complexes with glutamate dehydrogenase. *Eur. J. Biochem*. 1981;115:217-226.
28. Koberstein R, Sund H. The influence of ADP, GTP and L-glutamate on the binding of the reduced coenzyme to beef-liver glutamate dehydrogenase. *Eur. J. Biochem*. 1973; 36:545-552.

ACKNOWLEDGEMENTS

We gratefully acknowledge the Robert A. Welch Foundation (H-0037), the National Institutes of Health (GM-037657) for partial support of this work. This work used the Extreme Science and Engineering Discovery Environment (XSEDE), which is supported by National Science Foundation grant number ACI-1548562. The authors also acknowledge the Texas Advanced Computing Center (TACC) at The University of Texas at Austin for providing HPC resources that have contributed to the research results reported within this paper. URL: <http://www.tacc.utexas.edu>. The revised coordinates for bovine GDH complexed with NADH/Glu/GTP (6DHD), ADP (6DHK), ECG/NADPH (6DHL), Zn^{2+} (6DHM), Eu^{3+} (6DHN), and NADPH/Glu/GTP (6DHQ) have been deposited in the Protein Data Bank.

CONFLICT OF INTEREST

The authors declare no conflicts of interest with this work.

Chapter 4

Allosteric Discrimination at the NADH/ADP Regulatory Site of Glutamate Dehydrogenase

Omneya M. Nassar¹, Ka-Yiu Wong², Gillian Lynch², Thomas J. Smith², B. Montgomery
Pettitt^{*1, 2}

¹Department of Pharmacology and Toxicology, ²Department of Biochemistry and Molecular Biology, University of Texas Medical Branch, 301 University Blvd, Galveston, TX, 77555-0304

***Corresponding Authors:**

B. Montgomery Pettitt

Tel: 409-772-0723

Email: mpettitt@utmb.edu

Running Title: NADH and ADP binding to GDH allosteric site.

Total number of manuscript pages: 23

Number of Tables: 3

Number of Figures: 6

ABSTRACT

Glutamate dehydrogenase (GDH) is a target for treating insulin related disorders, such as hyperinsulinism hyperammonemia syndrome (HHS). Modeling native ligand binding at the NADH/ADP binding site has shown promise in designing GDH inhibitors and activators. Our computational investigation of the NADH/ADP site presented in this paper provides insight into the opposite allosteric effects of binding inhibitor NADH versus activator ADP to GDH. The computed binding free energy difference between NADH and ADP using thermodynamic integration is -0.3 kcal/mol, which is within the -0.275 and -1.7 kcal/mol experimental binding free energy difference range. Our simulations show a model of ADP inducing the open conformation of GDH (activation) and NADH promoting the closed conformation of GDH (inactivation), which supports previous experimental observations and provides more detail for hypotheses. The structural analysis of the important residues in the NADH/ADP binding site presented in this paper may provide potential targets for mutation studies for allosteric drug design.

INTRODUCTION

The role of glutamate dehydrogenase (GDH) in disease has been extensively studied and shown to be involved in some forms of the hyperinsulinism hyperammonemia syndrome (HHS)^{1, 2}. Point mutations in a number of residues in and around the binding site of the major GDH inhibitor, guanosine triphosphate (GTP)³⁻⁷ leads to uncontrolled catabolism of glutamate. There are also a number of HHS mutations located outside the GTP binding site, particularly in the antenna region, that also affect allosteric regulation of GDH.² This increased activity of mutant GDH leads to excess insulin secretion and accumulation of ammonium in HHS patients^{8, 9}.

GDH catalyzes the reversible oxidative deamination of glutamate to 2-oxoglutarate in the presence of coenzyme nicotinamide adenine dinucleotide (NAD(H)) or nicotinamide adenine dinucleotide phosphate (NADP(H))¹⁰. In HHS, the increased production of 2-oxoglutarate feeds into the Krebs cycle, stimulating adenosine triphosphate (ATP) production, and increasing insulin secretion from β -cells in the islets of Langerhans of the pancreas^{8, 9}. Thus, dysregulated GDH activity leads to excess insulin secretion and hypoglycemia in HHS patients. In addition, HHS depletes glutamate that is necessary to produce the important urea cycle intermediate N-acetylglutamate, resulting in the accumulation of ammonium^{8, 9}. Mammalian GDH is allosterically regulated by several metabolites that are indicative of cellular energy levels including adenosine diphosphate (ADP), NADH and GTP^{7, 10-12}. Therefore, under normal physiological conditions in mammals, GDH functions as an energy sensor of the pancreatic cell and correspondingly increases or decreases insulin secretion^{8, 9, 13, 14}.

The major allosteric inhibitor of GDH is GTP that binds to an allosteric site above the catalytic mouth at the base of the antenna of mammalian GDH^{7, 15}. GTP binding stabilizes closing of the catalytic mouth and prevents product release (the rate limiting

step)^{7, 15}. In contrast to GTP, ADP allosterically activates GDH by binding to the NADH/ADP binding site, abrogating GTP binding^{16, 17}. The NADH/ADP binding site is beneath the pivot helix, behind the catalytic cleft¹⁵⁻¹⁷. ADP binding facilitates the opening of the catalytic mouth, as seen in X-ray crystal structures¹⁸, thereby promoting product release as observed in binding and kinetic studies^{10, 19}. In addition to the active site, coenzyme NADH can bind to a secondary site, the NADH/ADP binding site, and enhances GTP inhibition of GDH activity by slowing product release^{17, 20}.

GDH can function as a soft-polymer of hexamers or as individual hexameric units in the mitochondrial matrix²¹. The GDH hexamer is a dimer of homotrimers with approximately 500 amino acids per monomer^{15-17, 22-25}. GDH structures show that each monomer has a GTP binding site as well as an NADH/ADP binding site, thus, each GDH hexamer can bind six GTP molecules, six ADP molecules, and six NADH molecules at their respective allosteric binding sites. GDH functionality has been associated experimentally with the hexameric form²⁶, but for computational expedience, the GDH trimer was utilized in our previous¹⁷ and current studies. Figure 4.1 shows the structure of the GDH trimer and with NADH bound to the NADH/ADP binding site.

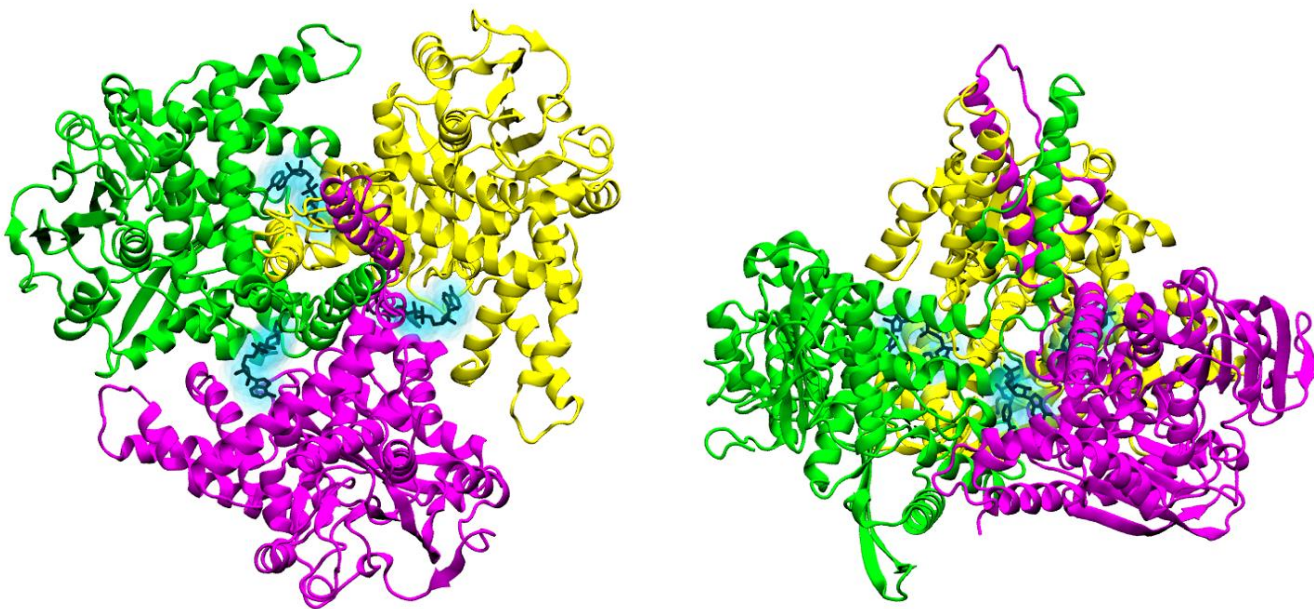


Figure 4.1: Structure of GDH in the trimeric form bound to three NADH molecules at the NADH/ADP binding site. Top view is on the right and side view is on the left. Each monomer is colored magenta, green or yellow. NADH molecules are colored in black and highlighted in light blue.

While the role of GDH in several diseases have been elucidated, developing agonists and antagonists to target GDH remains a challenge because of its complex regulation^{6,7}. There are several models and theories discussing the mechanism of GDH activation and inhibition, but they have yet to be validated experimentally¹⁷. The X-ray structures of wild type GDH in the open conformation and closed conformation as well as GDH mutant structures have been determined^{15-17, 22-25}. In addition, many of the structures that initially were determined using the incorrect protein sequence have been updated with the correct sequence and showed improved electron density of the NADH/ADP/ECG binding site¹⁷. This allosteric site is of particular importance since it binds both activators (ADP¹⁶ and presumably the synthetic activator 75-E10⁷) and

inhibitors (NADH⁵ and the green tea polyphenol, EGCG/ECG¹⁵). It is not at all clear how these different ligands can cause opposite effects by binding to the same site.

To better understand this complex regulatory site, the computational free energy technique thermodynamic integration (TI)²⁷ was used to compute the relative binding free energy difference of NADH versus ADP binding to GDH. The free energies presented in this article were calculated using TI. Free energies calculated using free energy perturbation (FEP)²⁸ are included in the supplemental information section. The conformational changes and free energy difference going from the GDH inhibited state (NADH bound) to the GDH activated state (ADP bound) were modelled.

METHODS

Software

Nanoscale Molecular Dynamics (NAMD) version 2.10²⁹ was used for running molecular dynamics simulations and Visual Molecular Dynamics (VMD) ³⁰ version 1.9.3 was employed for analysis of the trajectories. PROPKA 3.1³¹ in PlayMolecule³² was used to determine the protonation state of GDH at pH = 7 and the psfgen, solvate and autoionize plugins in VMD were used for further preparation of the systems.

Ligand System (ΔG_3 Computation)

For the solute in solution leg of the cycle one NADH molecule was transformed into one ADP molecule using the dual topology paradigm^{33, 34}. This aqueous system consisted of the solute molecule (PDB ID: 6DHD) placed in a 39Å x 39Å x 39Å cubic water box with 0.1 M NaCl. An NPT ensemble using a Langevin barostat and Langevin thermostat was employed. The integration time step was 2fs. Minimization of the system involved three stages utilizing the conjugant gradient method: 1) fixing the ligands and minimizing the solvent for 40,000 steps, 2) fixing the solvent and minimizing the ligand for 2,200 steps, and 3) minimizing the entire system for 40,000 steps. This process is used before equilibration of the system. Each of the 16 lambda intermediates was minimized (without fixing atoms) for 2,000 steps, equilibrated for 2 ns and run for 18 ns per intermediate. A total of 288 ns was run for the entire free energy path. Simulations were run in a NPT ensemble at 300K and 1 atm with TIP3P explicit solvent model.³⁵

Protein-Ligand Complex System (ΔG_1 Computation)

Using PROPKA 3.1 on PlayMolecule, GDH was protonated for a solution pH of 7. The GDH homotrimer was complexed with three ligand molecules: one ligand per NADH/ADP binding site. The system was placed in a 121Å x 121Å x 121Å cubic water box with 0.1M NaCl. The starting structure used was the GDH-NADH bound complex

(PDB ID: 6DHD) because the x-ray structure was determined to higher resolution. The simulation began with NADH and ended with ADP. Thus, the simulation involved the gradual transformation of NADH to ADP at the NADH/ADP binding sites. The sampling methods used for the small system was also used for the large system, except that each lambda intermediate was equilibrated for ~5 ns and run for 23 ns instead of 18 ns to achieve better convergence. Thus, the total set of trajectories was 368 ns. Simulations were run in a NPT ensemble at 300K and 1 atm with TIP3P explicit solvent model.³⁵

Free Energy Calculations

Free energies were calculated using thermodynamic integration (TI). The Hummer et al. correction³⁶ was added for the finite size effects of changing the charge of the ligand (-2 to -3) using Particle Mesh Ewald (PME) for the long-range electrostatic calculations. Equations 1 and 2 show the formulas for calculating TI and Hummer et al. correction, respectively. Free energies computed using TI were integrated using the 3/8 Simpson's method. Also, it is important to note that the lengths used to compute the Hummer et al. correction (L=39Å and L=121Å) are approximate average lengths and that the length of the simulation fluctuated in the NPT system.

$$\Delta G_i = \int_i^{i+1} \left\langle \frac{\partial U(\lambda)}{\partial \lambda} \right\rangle_\lambda d\lambda \quad (1)$$

$$\Delta G_{\text{correction}} = -\frac{1}{2} \zeta_{\text{Ewald}} (q_1^2 - q_0^2) \times 332 \quad (2)$$

RESULTS AND DISCUSSION

Binding Free Energy Calculation

Free energy changes presented in this paper were computed using TI (see supplemental information for computations calculated using FEP). The binding free energy ΔG_1 is equal to -50.90 kcal/mol (ΔG_1 per binding site is -16.97 kcal/mol) and is comparable to \sim -20 kcal/mol association free energy of ADP-protein binding studies.³⁷ The alchemical free energy change ΔG_3 is equal to -14.64 kcal/mol and is comparable to the reported -12 kcal/mol³⁸ and -16.3 kcal/mol³⁹ solvation free energies of adenine. The binding free energy difference computed ($\Delta\Delta G_{TI} = -0.3 \pm 1.882$ kcal/mol; see Table 4.1 and Figure 4.3) was within to the experimental binding free energy difference range ($\Delta\Delta G = -0.28$ to -1.7 kcal/mol; see Table 4.1).^{13, 19} Figure 4.2 shows the free energies at each intermediate for ΔG_1 and ΔG_3 .

The errors were calculated using the block standard error (BSE) method³⁴ with a block size of 1000. The maximum errors for ΔG_1 and ΔG_3 were ± 0.317 and ± 0.471 kcal/mol respectively. The standard square root of the sum of each window's variance for ΔG_1 and ΔG_3 were ± 0.963 and ± 1.882 kcal/mol respectively. A more conservative propagation of errors taken as the sum of the 16 window errors is shown in Table 4.2.

Experimental Binding Constants		Experiment (kcal/mol)	TI (kcal/mol)
K_D NADH	K_D ADP	$\Delta\Delta G_{exp}$	$\Delta\Delta G_{TI}$
$57 \times 10^{-6} M^a$	$3 \times 10^{-6} M^a$	-1.7	-0.3
$57 \times 10^{-6} M^a$	$35 \times 10^{-6} M^b$	-0.275	

Table 4.1: Computed binding free energy differences compared to experimental binding free energy differences. ^a Koberstein, R. and Sund, H., 1973¹⁹. ^b Frieden, C. 1959.⁴¹

λ window	$\Delta G_1(\lambda)$ (kcal/mol)	$\Delta G_3(\lambda)$ (kcal/mol)
total	0.963	1.882
0 to 0.0625	0.317	0.471
0.0625 to 0.125	0.153	0.214
0.125 to 0.1875	0.142	0.121
0.1875 to 0.25	0.127	0.175
0.25 to 0.3125	0.110	0.121
0.3125 to 0.375	0.102	0.127
0.375 to 0.4375	0.093	0.138
0.4375 to 0.5	0.063	0.107
0.5 to 0.5625	0.142	0.167
0.5625 to 0.625	0.189	0.217
0.625 to 0.6875	0.200	0.267
0.6875 to 0.75	0.240	0.181
0.75 to 0.8125	0.183	0.219
0.8125 to 0.875	0.213	0.254
0.875 to 0.9375	0.197	0.344
0.9375 to 1	0.311	0.418

Table 4.2: Total error and errors per lambda window for ΔG_1 and ΔG_3 calculated using the block standard error method.

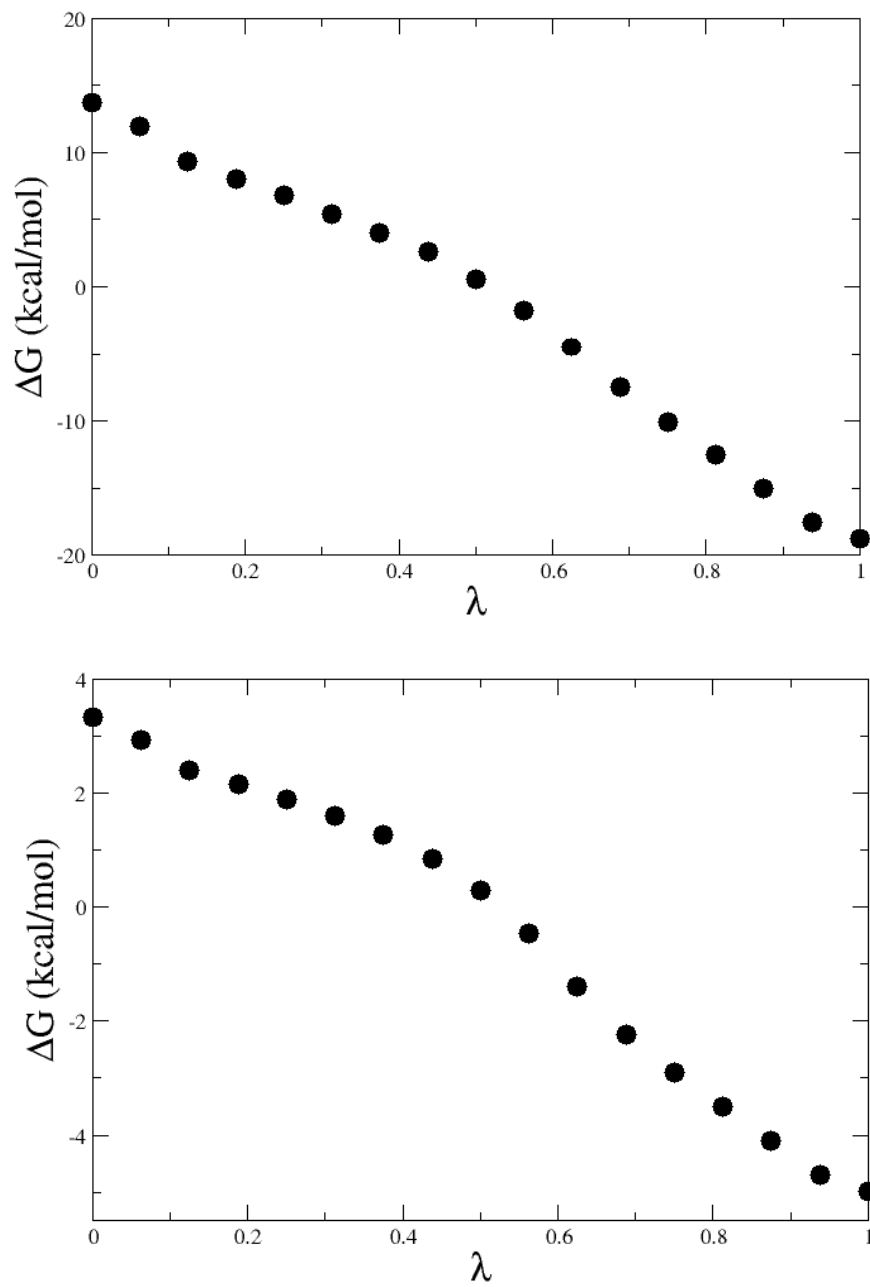


Figure 4.2: Free energy calculations using thermodynamic integration (TI) per λ intermediate for ΔG_1 (top) and ΔG_3 (bottom).

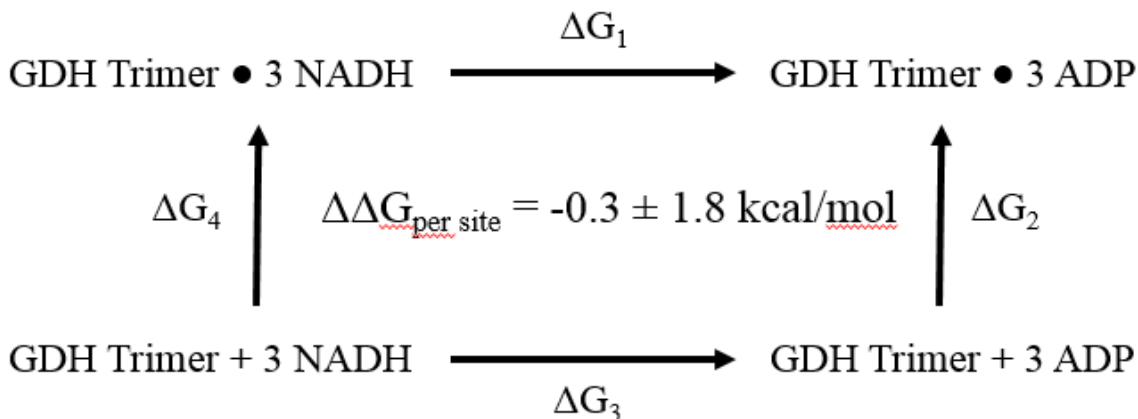


Figure 4.3: Computed relative binding free energy difference, $\Delta\Delta G$, of the alchemical conversion of NADH to ADP bound and unbound to GDH using TI is equal to -0.3 kcal/mol . Note that $\Delta\Delta G = \Delta G_1 - \Delta G_3 = \Delta G_2 - \Delta G_4$.

Structural Analysis of Conformational Changes

Figure 4.4 shows the catalytic motion of GDH, specifically in its trimeric form. The catalytic mouth in the closed position is shown in light blue while the open position is shown in orange. The mouth rotates approximately 18° between the open and closed state. The core region is colored in red and is typically bound to a core region of a second trimer (the GDH hexameric form is a dimer of trimers). However, the GDH trimer used is solvent exposed and lacks some protein-protein interactions found in the hexameric form.

The root-mean-squared-deviation (RMSD) of the open conformation (PDB ID: 6DHK) versus closed conformation (PDB ID: 6DHD) was compared to the GDH-Ligands trajectories and the crystallographic structures^{5, 18}. Opening of the catalytic mouth was observed in the GDH trimer/3ADP complex at the end state ($\lambda=1$; see Table 3). The conformation of the end GDH state diverges from the closed conformation by $\sim 3\text{\AA}$ and approaches the open conformation by $\sim 1.5\text{\AA}$. To further investigate the conformational changes of GDH, the RMSD was determined for the regions of the protein that have been identified as catalytically important and specified in Table 3.

Table 4.3 shows the RMSD of the crystallographic open conformation as well as the conformations from the simulations relative to the closed conformation. The regions that deviate greater than 3Å are the catalytic mouth (residues 250 to 350) and the antenna region (residues 440 to 448), specifically the flexible loop (residues 418 to 425) and pig tail regions (425-448). As expected, the core region has increased flexibility due to increased protein-solvent interactions that are typically restricted by protein-protein interactions in the hexameric form. In addition, the catalytic mouth opens significantly, but rarely completely based on the 3.5Å resolution X-ray structure (PDB ID: 6DHK)¹⁶.

This is an exciting result since it appears to agree with the proposed models for GDH activation and inhibition. During each catalytic cycle, the NAD binding domain of the catalytic mouth closes down upon the substrate and coenzyme. After catalysis, this domain opens to release the products and begin the catalytic cycle again. Therefore, activators such as ADP cannot ‘lock’ the enzyme into a particular conformational state but rather facilitates the slowest step of the reaction, NAD domain movement and product release. The corollary is that inhibitors, such as GTP and NADH, act in the opposite manner and make the NAD binding domain more difficult to move. These simulations show suggest that ADP facilitates the opening of the catalytic cleft while the NADH bound complex favors the closed state.

	Core	Catalytic Mouth	Antenna Region			
			Antenna	Flexible Loop	Pig Tail	Pivot Helix
Residues	50 - 175	250 - 350	400 - 418	418 - 425	425 - 448	448 - 475
RMSD (Å) Crystals	2.04	6.70	1.90	4.72	3.41	1.70
Average RMSD (Å) Trajectory	1.84	4.06	0.986	2.28	1.98	1.47
Maximum RMSD (Å) Trajectory	3.63	6.82	1.77	4.66	2.90	2.187

Table 4.3: RMSD comparison of crystallographic GDH open conformation (pdb 6DHK) and simulation relative to GDH closed conformation (pdb 6DHD) at different regions of GDH. RMSD crystals refers to the difference between the open and closed crystal forms^{5, 16}. Average refers to the difference between the experimental ADP structure and that averaged over the $\lambda=1$ trajectory. Maximum refers to the difference between the experimental ADP structure and that of the maximum deviation over the $\lambda=1$ trajectory.

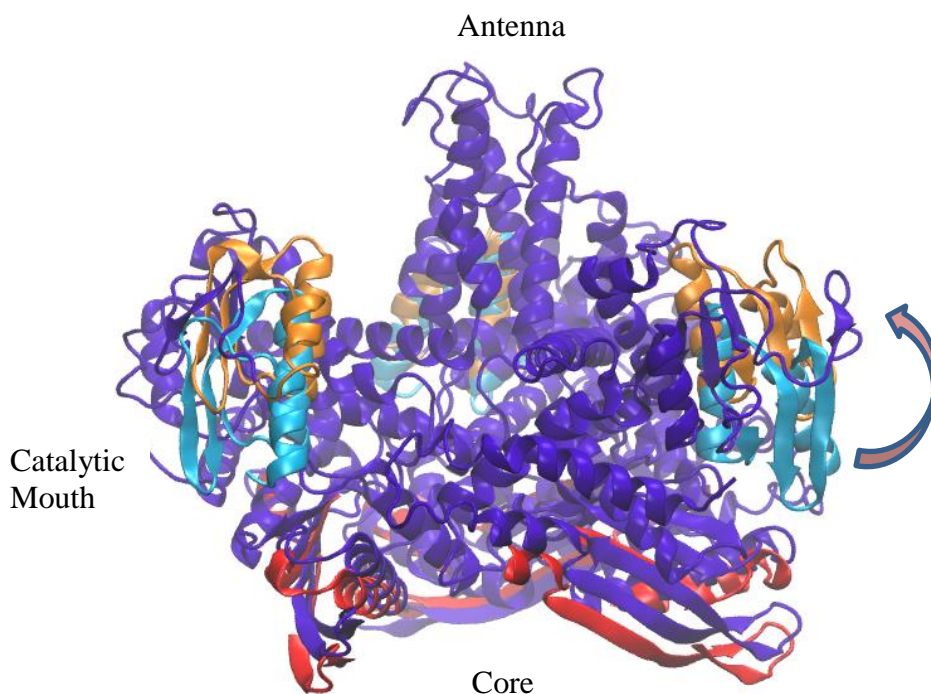


Figure 4.4: RMSD comparison of crystallographic GDH open (orange) conformation (PDB ID: 6DHK) relative to GDH closed (cyan) conformation (PDB ID: 6DHD). In purple is the GDH trimer in the closed conformation and in red is the core region in the open conformation, which is solvent exposed in our simulations.

ADP BINDING AT THE NADH/ADP SITE

Our simulations agree with crystallographic studies¹⁷ in that residues K387, R396, H209, R459, R491, D119, V120, R86 and H85 are involved in ADP binding. However, the interaction of these residues varied at each site, with the exception of V120 and H85 that always interacted with the adenine purine ring. At one ADP site, R491 interacts with the α and β phosphate groups while D119 interacts with the 2' hydroxyl group of the ribose and R86 interacts with the ribose ether oxygen. This is different from previously suggested contacts in which R491 appeared to interact with the ribose hydroxyl groups, D119 appeared to interact with the γ phosphate and R86 was appeared to interact with 2' hydroxyl group. The second NADH/ADP site in the trimer shows a different ADP-GDH interaction, one that better resembles the suggested interactions. Residues R396, R459, K387 and H209 interact with the β phosphate and R86 interacts with the ribose ether oxygen. R459 moves toward the β phosphate as the catalytic mouth opens, thereby possibly stabilizing the open conformation. The 2' hydroxyl group on the ribose interacts with D119 for 14ns then moves to interact with R491. The third NADH/ADP site shows the same β phosphate interactions with residues H209, R459, K387, and R396; however, D119 and R491 both interact with the 2' hydroxyl group on the ribose. It is important to note that both crystal observations and our molecular dynamics models show each monomer varying in NADH/ADP binding site conformation as well as varying in the degree the catalytic mouth opens. Figure 4.5 shows each ADP binding site with their respecting ligand-protein interactions.

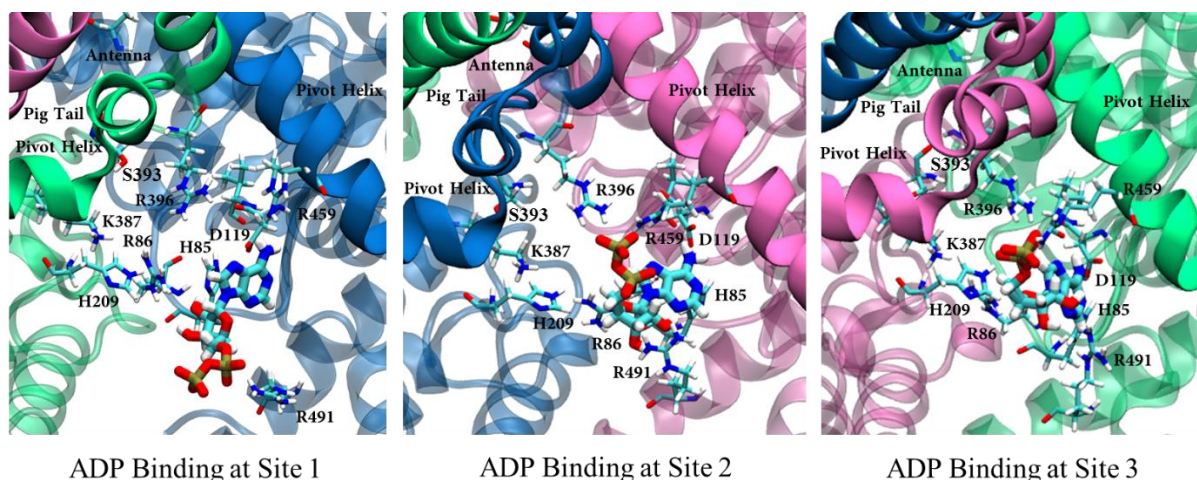


Figure 4.5: ADP interactions at each NADH/ADP binding site.

NADH BINDING AT NADH/ADP SITE

We can analyze the first and last windows of the thermodynamic integrations as unconstrained molecular dynamics of the respective systems. The residues involved in NADH binding include K387, H209, D119, R86, H85, V120, H195, I192, H391, T87, N388, and Y382 (all make contact with NADH except for Y382). The residues that interact with the nicotinamide group are H195, I192, H195, H391 and N388. The delta amine on H195 interacts with the ribose hydroxyl; this interaction lasts for 20 ns. The carbonyl oxygens on I192 and T87 interact with the nicotinamide amine group. The hydroxyl group on T87 also interacts with the nicotinamide amine. During the last 3ns of the simulation, the amine on the nicotinamide moves to interact with the delta amine on H391. The amine on N388 interacts with O2' hydroxyl group (2-3Å distance) and O3' hydroxyl group (3-4Å distance) for ~20ns. Although Y382 does not directly interact with NADH, it appears that the Y382 hydroxyl stabilizes the position of H391 by interacting with the H391 carbonyl for the entire 23ns trajectory. See Figure 4.6 below for the residue contacts with NADH at the NADH/ADP site.

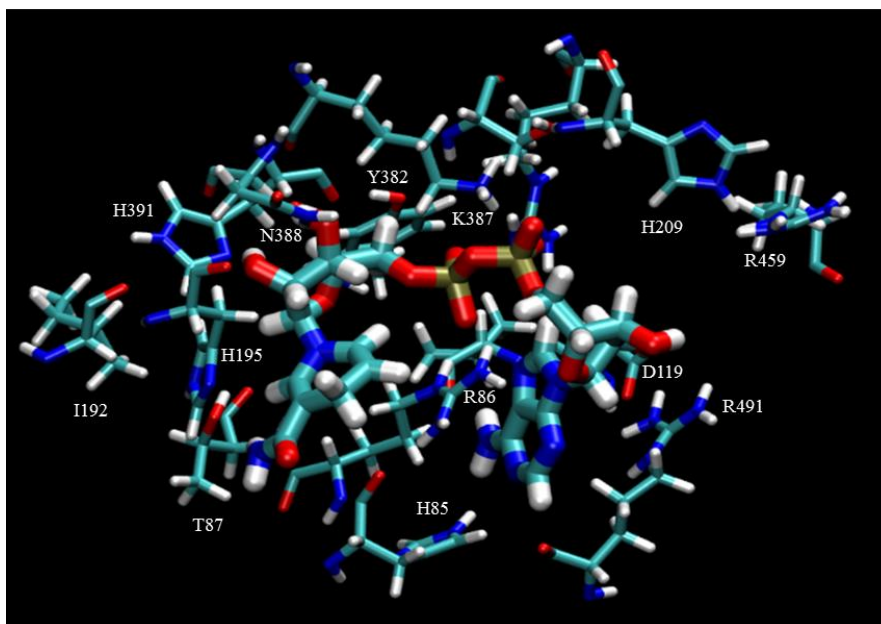


Figure 4.6: NADH binding at the NADH/ADP site.

The residues that contact the adenosine moiety of NADH include K387, H209, D119, R86, H85 and V120. Residue D119 carboxyl side chain maintains a close interaction (1-2Å) with O2' hydroxyl group throughout the trajectory while H85 and V120 maintain contact with the adenine group similar to ADP binding. K387 moves 2Å to maintain a close contact with the nicotinamide phosphates for the entire trajectory. In contrast, H209 remains distant for ~20 ns then moves to interact with NADH phosphates for the last 3ns. R86 begins by making contact and interacting with the NADH phosphates for ~9ns then moves ~7-9Å away. Residues R459, R491, and R396 remain distant from NADH, which contrasts with ADP binding. It appears that the increase in charge from -2 on NADH to -3 on ADP allows for increased duration and number of interactions of the phosphate moiety with GDH, specifically with residues R459, R491, H209, and R396.

Contrary to previous interpretations of the X-ray crystal structures¹⁷, S393 does not appear to favor ADP interactions in our simulations. Instead, it appears that the S393 hydroxyl group interacts with the E445 carboxyl group. This phenomenon is observed for

both ligands in both of our NADH-GDH and ADP-GDH simulations. E445 is located on the pivot helix, connecting the pivot helix to the pigtail region and S393 is located on a disordered region directly connected to the end of the antenna. The interaction between E445 and S393 limits the flexibility of the disordered region where S393 is located and is present in both the closed and open conformation. Thus, this interaction may be important for both the closed and open conformation possibly explaining why an S393I mutation results in loss of both GTP and ADP regulation. The position of E445 in close proximity to S393 is preserved by the ionic interaction between the carboxyl group on E445 and the amine group on K387.

CONCLUSION

Our computational analyses show comparable results to the crystallographic results with regard to the open and closed conformations in the presence of ADP and NADH, respectively, as well as reproduction of the binding free energy difference. The $\Delta\Delta G$ produced by TI of -0.3 kcal/mol is close to the experimental $\Delta\Delta G$ of -0.275 to -1.7 kcal/mol while ΔG_1 and ΔG_3 values were comparable to previous adenine binding and solvation free energies. These results are encouraging and the detailed analysis of the conformational changes leads to insight into the cooperative motions of GDH upon ligand binding. Future directions will include computing $\Delta\Delta G$ utilizing a potential of mean force to guide the conformation from the inhibited state (NADH bound) to the activated state (ADP bound).

ACKNOWLEDGEMENTS

We gratefully acknowledge the Robert A. Welch Foundation (H-0037), the National Institutes of Health (GM-037657) for partial support of this work. This work used the Extreme Science and Engineering Discovery Environment (XSEDE), which is supported by National Science Foundation grant number ACI-1548562. The authors also acknowledge the Texas Advanced Computing Center (TACC) at The University of Texas at Austin for providing HPC resources that have contributed to the research results reported within this paper. URL: <http://www.tacc.utexas.edu>.

CONFLICT OF INTEREST

The authors declare no conflicts of interest with this work.

REFERENCES

1. Palladino AA, Stanley CA. The hyperinsulinism/hyperammonemia syndrome. *Rev Endocr Metab Disord*. 2010;11:171-178.
2. Stanley CA, Lieu YK, Hsu BY, et al. Hyperinsulinism and hyperammonemia in infants with regulatory mutations of the glutamate dehydrogenase gene. *N Engl J Med*. 1998;338:1352-1357.
3. Li M, Li CH, Allen A, Stanley CA, Smith TJ. The structure and allosteric regulation of mammalian glutamate dehydrogenase. *Archives of Biochemistry and Biophysics*. 2012;519:69-80.
4. Smith HQaS, T.J. Identification of a novel activator of mammalian glutamate dehydrogenase. *Biochemistry*. 2016;55:8.
5. Peterson PE, Smith TJ. The structure of bovine glutamate dehydrogenase provides insights into the mechanism of allostery. *Structure*. 1999;7:769-782.
6. Smith TJ, Stanley CA. Untangling the glutamate dehydrogenase allosteric nightmare. *Trends in biochemical sciences*. 2008;33:557-564.
7. Smith HQ, Li C, Stanley CA, Smith TJ. Glutamate Dehydrogenase, a Complex Enzyme at a Crucial Metabolic Branch Point. *Neurochem Res*. 2017.
8. MacMullen C, Fang J, Hsu BY, et al. Hyperinsulinism/hyperammonemia syndrome in children with regulatory mutations in the inhibitory guanosine triphosphate-binding domain of glutamate dehydrogenase. *J Clin Endocrinol Metab*. 2001;86:1782-1787.
9. Weinzimer SA, Stanley CA, Berry GT, Yudkoff M, Tuchman M, Thornton PS. A syndrome of congenital hyperinsulinism and hyperammonemia. *J Pediatr*. 1997;130:661-664.
10. Frieden C. Glutamate Dehydrogenase. VI. Survey of Purine Nucleotide and Other Effects on the Enzyme From Various Sources. *The Journal of biological chemistry*. 1965;240:2028.
11. C. F. Glutamic dehydrogenase I. The effect of coenzyme on the sedimentation velocity and kinetic mechanism. . *Journal of Biological Chemistry*. 1959;234:809-814.

12. Bailey J BE, Bell JE. Regulation of bovine glutamate dehydrogenase. The effects of pH and ADP. . *Journal of Biological Chemistry*. 1982;257:5579-5583.
13. Stanley CA. Hyperinsulinism in infants and children. *Pediatr Clin North Am*. 1997;44:363-374.
14. Snider KE, Becker S, Boyajian L, et al. Genotype and Phenotype Correlations in 417 Children With Congenital Hyperinsulinism. *Journal of Clinical Endocrinology & Metabolism*. 2013;98:E355-E363.
15. Smith TJ, Peterson, P.E., Schmidt, T., Fang, J. and Stanley, C.A. Structures of bovine glutamate dehydrogenase complexes elucidate the mechanism of purine regulation. *Journal of molecular biology*. 2001;307:13.
16. Banerjee S, Schmidt, T., Fang, J., Stanley, C.A. and Smith, T.J. Structural studies on ADP activation of mammalian glutamate dehydrogenase and the evolution of regulation. *Biochemistry*. 2003;42:10.
17. Nassar OM, Li C, Stanley CA, Pettitt BM, Smith TJ. Glutamate dehydrogenase: Structure of a hyperinsulinism mutant, corrections to the atomic model, and insights into a regulatory site. *Proteins*. 2018.
18. Banerjee S, Schmidt T, Fang J, Stanley CA, Smith TJ. Structural studies on ADP activation of mammalian glutamate dehydrogenase and the evolution of regulation. *Biochemistry*. 2003;42:3446-3456.
19. Koberstein R, Sund H. Studies of glutamate dehydrogenase. The influence of ADP, GTP, and L-glutamate on the binding of the reduced coenzyme to beef-liver glutamate dehydrogenase. *Eur J Biochem*. 1973;36:545-552.
20. Smith TJ, Peterson PE, Schmidt T, Fang J, Stanley CA. Structures of bovine glutamate dehydrogenase complexes elucidate the mechanism of purine regulation. *Journal of molecular biology*. 2001;307:707-720.
21. Frieden C, Colman RF. Glutamate dehydrogenase concentration as a determinant in the effect of purine nucleotides on enzymatic activity. *J Biol Chem*. 1967;242:1705-1715.
22. Bailey J, Powell, L., Sinanan, L., Neal, J., Li, M., Smith, T. and Bell, E. A novel mechanism of V-type zinc inhibition of glutamate dehydrogenase results from disruption of subunit interactions necessary for efficient catalysis. *The FEBS Journal*. 2011;278:11.

23. Li M, Smith, C.J., Walker, M.T. and Smith, T.J. Novel Inhibitors Complexed with Glutamate Dehydrogenase: Allosteric Regulation by Control of Protein Dynamics. *Journal of Biological Chemistry*. 2009;284:12.
24. Borgnia MJ, Banerjee, S., Merk, A., Matthies, D., Bartesaghi, A., Rao, P., Pierson, J., Earl, L.A., Falconieri, V., Subramaniam, S. and Milne, J.L. Using cryo-EM to map small ligands on dynamic metabolic enzymes: studies with glutamate dehydrogenase. *Molecular Pharmacology*. 2016;89:6.
25. Merk A, Bartesaghi, A., Banerjee, S., Falconieri, V., Rao, P., Davis, M.I., Pragani, R., Boxer, M.B., Earl, L.A., Milne, J.L. and Subramaniam, S. Breaking cryo-EM resolution barriers to facilitate drug discovery. *Cell*. 2016;165:9.
26. Bell E, Bell JE. Catalytic activity of bovine glutamate dehydrogenase requires a hexamer structure. *Biochemical Journal*. 1984;217:327-330.
27. Straatsma TPaB, H.J.C. Free energy of ionic hydration: Analysis of a thermodynamic integration technique to evaluate free energy differences by molecular dynamics simulations. *The Journal of Chemical Physics*. 1988;89:5876-5886.
28. Zwanzig RW. High-temperature equation of state by a perturbation method. I. nonpolar gases. *The Journal of Chemical Physics*. 1954;22:1420-1426.
29. Phillips JC, Braun R, Wang W, et al. Scalable molecular dynamics with NAMD. *J Comput Chem*. 2005;26:1781-1802.
30. Humphrey W, Dalke A, Schulten K. VMD: visual molecular dynamics. *J Mol Graph*. 1996;14:33-38, 27-38.
31. Rostkowski M, Olsson MH, S ndergaard CR, Jensen JH. Graphical analysis of pH-dependent properties of proteins predicted using PROPKA. *BMC structural biology*. 2011;11:6.
32. Mart nez-Rosell G, Giorgino T, De Fabritiis G. PlayMolecule ProteinPrepare: A Web Application for Protein Preparation for Molecular Dynamics Simulations. *J Chem Inf Model*. 2017;57:1511-1516.
33. Pearlman DA. A comparison of alternative approaches to free energy calculations. *The Journal of Physical Chemistry*. 1994; 98:1487-1493.
34. Chipot C, Pohorille A, Harvard. *Free energy calculations*: Springer-Verlag Berlin Heidelberg; 2007.

35. Jorgensen WL, Chandrasekhar J, Madura JD, Impey RW, Klein ML. Comparison of simple potential functions for simulating liquid water. *The Journal of chemical physics*. 1983;79:926-935.
36. Hummer G, Pratt LR, Garcia AE. Free energy of ionic hydration. *The Journal of Physical Chemistry*. 1996;100:1206-1215.
37. Kawaguchi K, Saito, Hiroaki, Okazaki S, Nagao H. Molecular dynamics study on the free energy profile for dissociation of ADP from N-terminal domain of Hsp90. *Chemical Physics Letters*. 2013;588:226-230.
38. Miller JL, Kollman PA. Solvation free energies of the nucleic acid bases. *The Journal of Physical Chemistry* 1996;100:8587-8594.
39. Cornell WD, Cieplak P, Bayly CI, et al. A second generation force field for the simulation of proteins, nucleic acids, and organic molecules. *Journal of the American Chemical Society*. 1995; 117 5179-5197.
40. Grossfield A, Zuckerman DM. Quantifying uncertainty and sampling quality in biomolecular simulations. *Annual reports in computational chemistry*. 2009;5:23-48.
41. FRIEDEN C. Glutamic dehydrogenase. II. The effect of various nucleotides on the association-dissociation and kinetic properties. *J Biol Chem*. 1959;234:815-820.

SUMMARY AND FUTURE DIRECTIONS

As previously mentioned in the introduction, modeling ligand-GDH interactions can provide insight in therapeutic development to treat insulin related disorders, such as HHS. The work presented in this dissertation discusses important interactions between GDH with activator ADP and inhibitor NADH at the NADH/ADP binding site. Chapter 3 discusses the importance of residue 387, which was previously mistakenly identified as asparagine instead of lysine. The free energy penalty for the mistake of having asparagine instead of lysine at residue 387 would be +5 kcal/mol per binding site which would prevent the structures from being useful for computational drug design methods. The importance of having K387 is reinforced by our GDH-NADH and GDH-ADP models presented in Chapter 4. With the improved electron density of NADH and ADP at the NADH/ADP binding site after correcting residue 387 identity to lysine, we computationally modeled the binding of NADH and ADP to GDH. While small but important contributions were made to the field, there is always more to be done.

Additional studies to model native ligand binding to glutamate dehydrogenase include simulating S393I mutation to understand ADP and GTP binding as well as modeling GTP binding in wild type GDH and HHS mutant H454Y GDH. In our computational model of NADH and ADP binding to GDH, it was found that S393 was not involved in ADP binding even though experimental mutagenesis studies show that S393I results in loss of ADP and GTP regulation. While our computational studies do not show S393 interacting with ADP, we have yet to model GTP binding to GDH and observe potential interactions of S393 when GTP is bound. Modeling and comparing GTP versus ADP binding in the presence of S393I mutation can provide insight in conformational changes that occur or potential change in contacts with ligands such as GTP and ADP. Figure 5.1 shows the thermodynamic cycles we can use to model S393I

in the presence of GTP and ADP to understand loss of ligand binding due to the S393I mutation.

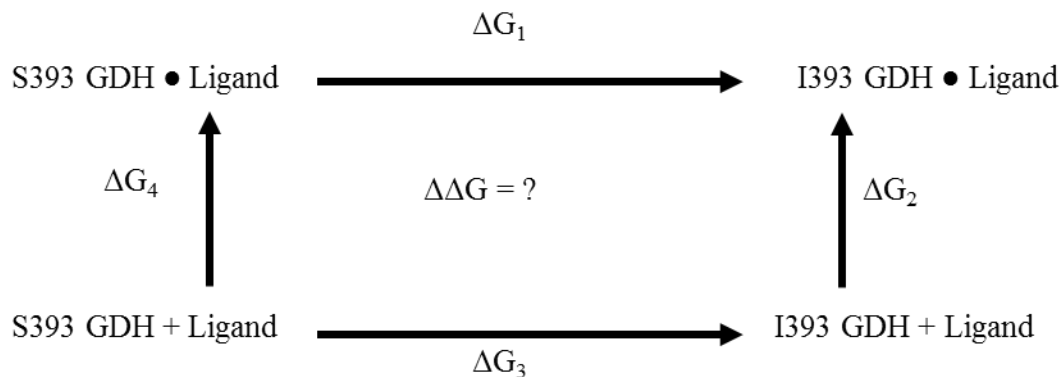


Figure 5.1: Thermodynamic cycle to compute free energy penalty of S393I mutation in the presence of a native ligand, such as ADP or GTP.

Figure 5.2 shows the thermodynamic cycles we can use to calculate the additional binding free energy values of ligand-GDH complexes. These cycles can be used to isolate and determine the favorable GTP binding conformations that agrees with the binding free energy values showing an increase affinity of GDH for substrate and cofactor binding. This is important to distinguish GTP binding and GTP inactivation. H454YGDH is mutant GDH found in HHS patients, K387GDH is wild-type GDH with the correct bovine GDH sequence (pdb 6DHD), and ApoGDH is the unbound GDH structure (pdb 1L1F). N387GDH is the original bovine GDH crystal structure that contains the wrong sequence and was previously discussed in Chapter 3. The reason it is important to observe ligand-GDH interactions in the presence or absence of NADHc (cofactor) and substrate (glutamate) is because the GTP mechanism of inhibition involves the increased affinity of the GDH enzyme for the cofactor and substrate binding induced upon GTP binding. Calculating the binding free energy of H454Y mutant interacting with GTP in the presence or absence of cofactor (NADHc) will demonstrate if the affinity for the

cofactor (NADHc) is decreased when GTP is bound. H454Y GDH mutant interacting with phosphate or GTP in the absence of NADHc and glutamate does not show if the binding affinity of mutant GDH for the cofactor (NADHc) and glutamate has changed. Thus, GDH interacting with regulatory ligands in the absence of cofactor and substrate only elucidates GTP binding and not GTP inactivation of GDH.

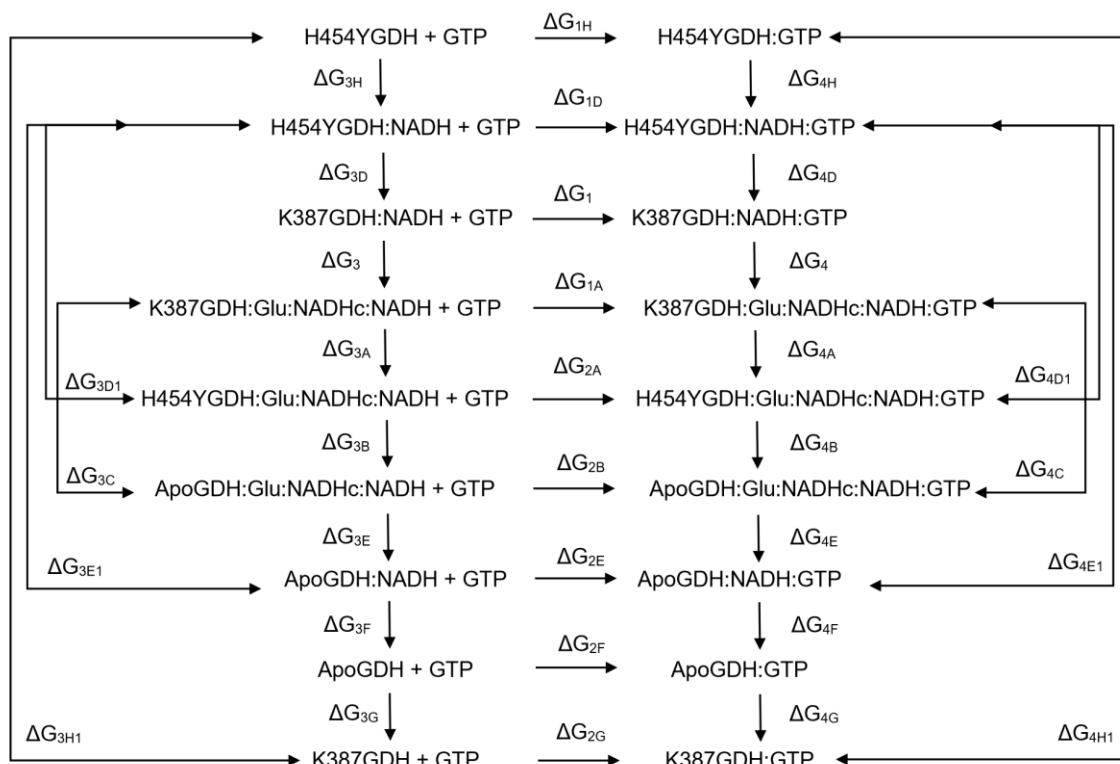


Figure 5.2: Thermodynamic Cycles Used to Calculate Binding Free Energy Differences ($\Delta\Delta G$).

The crystal structure of H454Y mutant GDH provided by Dr. Thomas J. Smith, (see Chapter 3) only contains phosphates and water molecules as floating ligands in the crystal structure: both the cofactor (NADHc) and substrate (glutamate) are not in the crystal structure. There are no available crystal structures of GDH containing a HHS mutation bound to the cofactor (NADHc) and substrate (glutamate) to our knowledge. Thus, H454Y may actually be in a conformational state that keeps the NAD binding domain open and does not favor the binding of cofactor (NADHc) and substrate

(glutamate). If the H454Y mutant GDH crystal is reflective of the disease HHS, then the activity of the enzyme should be increased and the affinity for the cofactor (NADHc) and substrate/product should decrease in order to increase product release. However, it is unclear whether the H454Y interaction with GTP decreases without a change of affinity for the cofactor and substrate. For example, computing the binding free energy difference of ΔG_1 and ΔG_{1A} in Figure 5.2 can show the discrepancy between GTP binding and GTP inactivation.

APPENDICIES

Appendix A

APPENDIX A1 : BLOCK STANDARD ERROR ANALYSIS OF BINDING FREE ENERGY CALCUATIONS (N = 1000) FOR ΔG_1 CALCULATION IN CHAPTER 3

ΔG_1 Errors (kcal/mol) (n=1000)

	ΔG_1 electrostatics	ΔG_1 van der Waals
Maximum Error	± 0.086	± 0.043
$\lambda = 0$ to $\lambda = 1/16$	± 0.029	± 0.025
$\lambda = 1/16$ to $\lambda = 2/16$	± 0.035	± 0.027
$\lambda = 2/16$ to $\lambda = 3/16$	± 0.025	± 0.021
$\lambda = 3/16$ to $\lambda = 4/16$	± 0.050	± 0.022
$\lambda = 4/16$ to $\lambda = 5/16$	± 0.067	± 0.020
$\lambda = 5/16$ to $\lambda = 6/16$	± 0.064	± 0.019
$\lambda = 6/16$ to $\lambda = 7/16$	± 0.086	± 0.020
$\lambda = 7/16$ to $\lambda = 8/16$	± 0.061	± 0.017
$\lambda = 8/16$ to $\lambda = 9/16$	± 0.055	± 0.014
$\lambda = 9/16$ to $\lambda = 10/16$	± 0.058	± 0.017
$\lambda = 10/16$ to $\lambda = 11/16$	± 0.039	± 0.023
$\lambda = 11/16$ to $\lambda = 12/16$	± 0.053	± 0.015
$\lambda = 12/16$ to $\lambda = 13/16$	± 0.048	± 0.011
$\lambda = 13/16$ to $\lambda = 14/16$	± 0.032	± 0.022
$\lambda = 14/16$ to $\lambda = 15/16$	± 0.039	± 0.019
$\lambda = 15/16$ to $\lambda = 1$	± 0.033	± 0.043

**APPENDIX A2 : BLOCK STANDARD ERROR ANALYSIS OF BINDING FREE ENERGY
CALCULATIONS (N = 1000) FOR ΔG_3 CALCULATION IN CHAPTER 3**

ΔG_3 Errors (kcal/mol) (n=1000)

	ΔG_3 electrostatics	ΔG_3 van der Waals
Maximum Error	± 0.047	± 0.046
$\lambda = 0$ to $\lambda = 1/16$	± 0.031	± 0.029
$\lambda = 1/16$ to $\lambda = 2/16$	± 0.035	± 0.023
$\lambda = 2/16$ to $\lambda = 3/16$	± 0.020	± 0.027
$\lambda = 3/16$ to $\lambda = 4/16$	± 0.047	± 0.025
$\lambda = 4/16$ to $\lambda = 5/16$	± 0.025	± 0.024
$\lambda = 5/16$ to $\lambda = 6/16$	± 0.034	± 0.022
$\lambda = 6/16$ to $\lambda = 7/16$	± 0.027	± 0.046
$\lambda = 7/16$ to $\lambda = 8/16$	± 0.047	± 0.036
$\lambda = 8/16$ to $\lambda = 9/16$	± 0.042	± 0.025
$\lambda = 9/16$ to $\lambda = 10/16$	± 0.032	± 0.020
$\lambda = 10/16$ to $\lambda = 11/16$	± 0.032	± 0.013
$\lambda = 11/16$ to $\lambda = 12/16$	± 0.026	± 0.018
$\lambda = 12/16$ to $\lambda = 13/16$	± 0.030	± 0.026
$\lambda = 13/16$ to $\lambda = 14/16$	± 0.029	± 0.029
$\lambda = 14/16$ to $\lambda = 15/16$	± 0.036	± 0.020
$\lambda = 15/16$ to $\lambda = 1$	± 0.028	0.039

**APPENDIX A3 : BLOCK STANDARD ERROR ANALYSIS OF BINDING FREE ENERGY
CALCULATIONS (N = 10000) FOR ΔG_1 CALCULATION IN CHAPTER 3**

ΔG_1 Errors (kcal/mol) (n=10000)

	ΔG_1 electrostatics	ΔG_1 van der Waals
Maximum Error	± 0.26	± 0.13
$\lambda = 0$ to $\lambda = 1/16$	± 0.059	± 0.058
$\lambda = 1/16$ to $\lambda = 2/16$	± 0.097	± 0.067
$\lambda = 2/16$ to $\lambda = 3/16$	± 0.054	± 0.051
$\lambda = 3/16$ to $\lambda = 4/16$	± 0.14	± 0.050
$\lambda = 4/16$ to $\lambda = 5/16$	± 0.20	± 0.043
$\lambda = 5/16$ to $\lambda = 6/16$	± 0.19	± 0.036
$\lambda = 6/16$ to $\lambda = 7/16$	± 0.26	± 0.040
$\lambda = 7/16$ to $\lambda = 8/16$	± 0.15	± 0.038
$\lambda = 8/16$ to $\lambda = 9/16$	± 0.14	± 0.029
$\lambda = 9/16$ to $\lambda = 10/16$	± 0.15	± 0.044
$\lambda = 10/16$ to $\lambda = 11/16$	± 0.073	± 0.067
$\lambda = 11/16$ to $\lambda = 12/16$	± 0.14	± 0.037
$\lambda = 12/16$ to $\lambda = 13/16$	± 0.14	± 0.020
$\lambda = 13/16$ to $\lambda = 14/16$	± 0.079	± 0.061
$\lambda = 14/16$ to $\lambda = 15/16$	± 0.072	± 0.039
$\lambda = 15/16$ to $\lambda = 1$	± 0.063	± 0.130

**APPENDIX A4 : BLOCK STANDARD ERROR ANALYSIS OF BINDING FREE ENERGY
CALCULATIONS (N = 10000) FOR ΔG_3 CALCULATION IN CHAPTER 3**

ΔG_3 Errors (kcal/mol) (n=10000)

	ΔG_3 electrostatics	ΔG_3 van der Waals
Maximum Error	± 0.13	± 0.12
$\lambda = 0$ to $\lambda = 1/16$	± 0.064	± 0.059
$\lambda = 1/16$ to $\lambda = 2/16$	± 0.082	± 0.051
$\lambda = 2/16$ to $\lambda = 3/16$	± 0.040	± 0.069
$\lambda = 3/16$ to $\lambda = 4/16$	± 0.13	± 0.049
$\lambda = 4/16$ to $\lambda = 5/16$	± 0.050	± 0.051
$\lambda = 5/16$ to $\lambda = 6/16$	± 0.092	± 0.055
$\lambda = 6/16$ to $\lambda = 7/16$	± 0.056	± 0.12
$\lambda = 7/16$ to $\lambda = 8/16$	± 0.13	± 0.081
$\lambda = 8/16$ to $\lambda = 9/16$	± 0.095	± 0.047
$\lambda = 9/16$ to $\lambda = 10/16$	± 0.068	± 0.047
$\lambda = 10/16$ to $\lambda = 11/16$	± 0.064	± 0.028
$\lambda = 11/16$ to $\lambda = 12/16$	± 0.057	± 0.050
$\lambda = 12/16$ to $\lambda = 13/16$	± 0.069	± 0.072
$\lambda = 13/16$ to $\lambda = 14/16$	± 0.068	± 0.076
$\lambda = 14/16$ to $\lambda = 15/16$	± 0.087	± 0.044
$\lambda = 15/16$ to $\lambda = 1$	± 0.062	± 0.10

Appendix B

APPENDIX B1: TABLES OF FREE ENERGY VALUES FOR ΔG_1 CALCULATION IN CHAPTER 4 USING TI.

Thermodynamic Integration

λ	ΔG_1	ΔG_1 per binding site
total	-50.90	-16.97
0	13.75	4.58
0.0625	11.92	3.97
0.1250	9.36	3.12
0.1875	8.02	2.67
0.2500	6.85	2.28
0.3125	5.45	1.82
0.3750	4.00	1.33
0.4375	2.59	0.86
0.5000	0.58	0.19
0.5625	-1.80	-0.60
0.6250	-4.52	-1.51
0.6875	-7.47	-2.49
0.7500	-10.06	-3.35
0.8125	-12.53	-4.18
0.9333	-15.01	5.00
0.9375	-17.53	-5.84
1	-18.81	-6.27

APPENDIX B2: TABLES OF FREE ENERGY VALUES FOR ΔG_1 CALCULATION IN CHAPTER 4 USING FEP.

Free Energy Perturbation

λ window	ΔG_1	ΔG_1 per binding site
total	-644.66	-214.89
0 to 0.0625	178.75	59.58
0.0625 to 0.125	147.17	49.06
0.125 to 0.1875	125.77	41.92
0.1875 to 0.25	107.36	35.79
0.25 to 0.3125	89.22	29.74
0.3125 to 0.375	62.86	20.95
0.375 to 0.4375	43.56	14.52
0.4375 to 0.5	20.87	6.96
0.5 to 0.5625	-25.88	-8.63
0.5625 to 0.625	-65.56	-21.85
0.625 to 0.6875	-118.26	-39.42
0.6875 to 0.75	-162.51	-54.17
0.75 to 0.8125	-199.91	-66.64
0.8125 to 0.875	-240.33	-80.11
0.875 to 0.9375	-282.85	-94.28
0.9375 to 1	-324.91	-108.30

APPENDIX B3: TABLES OF FREE ENERGY VALUES FOR ΔG_3 CALCULATION IN CHAPTER 4 USING TI (LEFT) AND FEP (RIGHT).

Thermodynamic Integration		Free Energy Perturbation	
λ	ΔG_3	λ window	ΔG_3
total	-14.64	total	-218.96
0	3.33	0 to 0.0625	41.73
0.0625	2.94	0.0625 to 0.125	34.99
0.1250	2.40	0.125 to 0.1875	31.93
0.1875	2.15	0.1875 to 0.25	28.00
0.2500	1.89	0.25 to 0.3125	23.61
0.3125	1.60	0.3125 to 0.375	18.91
0.3750	1.27	0.375 to 0.4375	12.70
0.4375	0.85	0.4375 to 0.5	5.85
0.5000	0.30	0.5 to 0.5625	-6.61
0.5625	-0.46	0.5625 to 0.625	-22.20
0.6250	-1.39	0.625 to 0.6875	-37.73
0.6875	-2.23	0.6875 to 0.75	-48.51
0.7500	-2.90	0.75 to 0.8125	-59.46
0.8125	-3.50	0.8125 to 0.875	-68.90
0.9333	-4.09	0.875 to 0.9375	-80.62
0.9375	-4.69	0.9375 to 1	-92.62
1	-4.98		

**APPENDIX B4: TABLES OF FREE ENERGY VALUES FOR ΔG_4 , ΔG_2 , ΔG_1 AND ΔG_3
(CHAPTER 4).**

Experimental Binding Constants		ΔG experimental (kcal/mol)			ΔG TI (kcal/mol)			ΔG FEP (kcal/mol)		
K_D NADH	K_D ADP	ΔG_4 NADH	ΔG_2 ADP	$\Delta\Delta G$	ΔG_1	ΔG_3	$\Delta\Delta G$	ΔG_1	ΔG_3	$\Delta\Delta G$
57×10^{-6} M^1	$3 \times 10^{-6} M^1$	-5.8	-7.5	-1.7	-75.6	-75.4	-0.3	-273.2	-279.4	6.20
	$35 \times 10^{-6} M^2$		-6.075	-0.275						

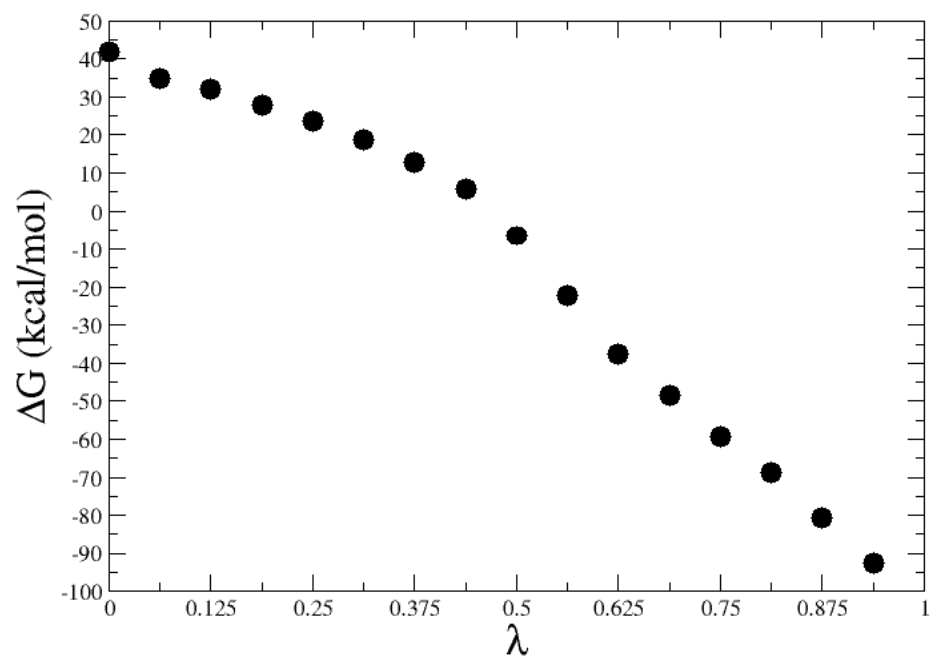
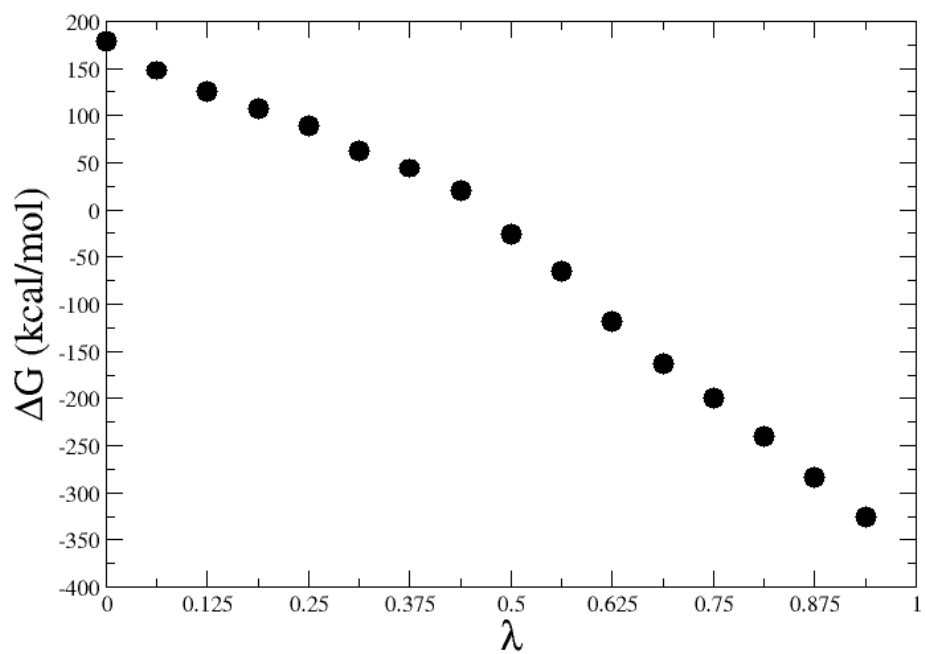
**APPENDIX B5: COMPUTATION OF HUMMER ET AL. CALCULATION FOR ΔG_1 AND ΔG_3
(CHAPTER 4).**

Hummer et al Correction Calculation				
Equation:	$(1/2)(-2.837)(332)(q_1^2 - q_0^2)/L$			
ΔG_1 correction	-175	$L = 121$	$q_1 = -3 \times 3$	$q_0 = -2 \times 3$
ΔG_3 correction	-60.4	$L = 39$	$q_1 = -3$	$q_0 = -2$

¹ Koberstein, R. and Sund, H., 1973. Studies of Glutamate Dehydrogenase: The Influence of ADP, GTP, and L-Glutamate on the Binding of the Reduced Coenzyme to Beef-Liver Glutamate Dehydrogenase. European Journal of Biochemistry, 36(2), pp 545-552.

² Koberstein, R. and Sund, H., 1973. Studies of Glutamate Dehydrogenase: The Influence of ADP, GTP, and L-Glutamate on the Binding of the Reduced Coenzyme to Beef-Liver Glutamate Dehydrogenase. European Journal of Biochemistry, 36(2), pp 545-552.

APPENDIX B6: FREE ENERGY CALCULATIONS USING FREE ENERGY PERTURBATION (FEP) PER λ INTERMEDIATE FOR $\Delta G1$ (TOP) AND $\Delta G3$ (BOTTOM) FOR CHAPTER 4.



The binding free energy difference obtained using FEP ($\Delta\Delta G_{\text{FEP}} = +6.20$ kcal/mol) deviated greatly from the experimental binding free energy difference. Because the free energy perturbation technique weighs rare conformations more heavily than thermodynamic integration, the free energy computed deviates greatly than free energies computed using the more common conformations. Free energies computed using thermodynamic integration reached convergence sooner than those computed using free energy perturbation. Thus, it may be possible that free energies computed using FEP could converge to TI results if simulations were left to run for longer and more potential energies were sampled.

The range in free energies is significantly different. FEP computed free energies ranged from -325 to 178 kcal/mol for ΔG_1 and -92 to 42 kcal/mol for ΔG_3 . TI computed free energies has smaller ranges with -18.81 to 13.75 kcal/mol for ΔG_1 and -4.98 to 3.33 kcal/mol for ΔG_3 .

Vita

Omneya Nassar was born in San Jose, California on December 19, 1990 to Mohamed Nassar (father) and Eyman Nassar (mother). She attended Linder Elementary School, Lively Middle School (previously known as Fulmore Middle School) and the Liberal Arts and Science Academy High School in Austin, Texas. She continued her studies in Austin and attained a Bachelors of Science degree in Biochemistry from St. Edward's University. There, she developed a passion for teaching and research as she worked as a supplemental instructor for general chemistry lecture and teaching assistant for organic chemistry, forensic chemistry, chemical instrumentation, and general chemistry labs while conducting research in the synthesis of biocompatible arylated guanosine gels. After rotating in Dr. B. Montgomery Pettitt's lab, she found that computational chemistry quenched her scientific curiosity and pursued her doctoral research in free energy calculations of ligand-glutamate dehydrogenase interactions.

Permanent address: 9308 Bernoulli Dr. Austin, TX 78748

This dissertation was typed by Omneya Nassar.